Cryptochrome-Timeless structure reveals circadian clock timing mechanisms

Changfan Lin[†], Shi Feng[†], Cristina C. DeOliveira and Brian R. Crane
[†]Equal Contribution

Department of Chemistry and Chemical Biology, Cornell University, Ithaca NY 14853

Circadian rhythms influence many behaviors and diseases[1,2]. They arise from oscillations in gene expression caused by repressor proteins that directly inhibit transcription of their own genes. The fly circadian clock offers a valuable model for studying these processes, wherein Timeless (TIM) plays a critical role in mediating nuclear entry of the transcriptional repressor Period (PER) and the photoreceptor Cryptochrome (CRY) entrains the clock by triggering TIM degradation in light[2,3]. The cryo-EM structure of the CRY:TIM complex reveals how a light-sensing cryptochrome recognizes its target. CRY engages a continuous core of N-terminal TIM armadillo (ARM) repeats, resembling how photolyases recognize damaged DNA, and binds a C-terminal TIM helix reminiscent of the interactions between light-insensitive CRYs and their partners in mammals. The structure highlights how the CRY flavin cofactor undergoes conformational changes that couple to large-scale rearrangements at the molecular interface, and how a phosphorylated segment in TIM may impact clock period by regulating the binding of importin-α and the nuclear import of TIM:PER[4,5]. Moreover, the structure reveals that the TIM N-terminus inserts into the restructured CRY pocket to replace the autoinhibitory C-terminal tail released by light, thereby providing a possible explanation for how the LS-TIM polymorphism adapts flies to different climates[6,7].

Circadian rhythms rely on cell-autonomous molecular clocks composed of transcriptional-translational feedback loops[1,2]. In the paradigm clock of *Drosophila melanogaster* (**Figure 1a**), the transcriptional repressor proteins Period (PER) and Timeless (TIM) associate and accumulate in the cytosol before timed transport to the nucleus where they inhibit the transcription factors Clock (CLK) and Cycle (CYC)[2,3] and thereby downregulate the expression of *per*, *tim* and other clock-controlled genes[2,3] (**Figure 1a**). A cascade of TIM phosphorylation by the SHAGGY (SGG) and CK2 kinases gates nuclear entry of PER:TIM to properly time the circadian oscillator[4]. TIM co-transports PER by binding directly to the nuclear import factor importin-α1[5].

The fly clock is entrained by the flavoprotein Cryptochrome (CRY, **Figure 1a**), which binds to TIM in the light (**Figure 1b**) and directs it for proteasomal degradation[2,3,8]. CRYs share a flavin-binding Photolyase Homology Region (PHR) with the DNA repair enzymes photolyase (PL) but also contain a CRY C-terminal extension (CCE) that is specific for the function of a given CRY[9-11]. Type I CRYs from plants and animals sense light to reset the circadian clock; Type II CRYs from mammalians repress transcription in a light-independent manner by binding the PER proteins and directly inhibiting CLK[9,10]. In Drosophila, photoreduction of the CRY FAD to the anionic semiquinone (ASQ) by a tryptophan tetrad (W342, W397, W420, W394) triggers release of a C-terminal tail (CTT) helix (**Figure 1b**)[12-15,16-18]. Photoreduced CRY resets TIM levels by binding TIM and recruiting the E3 ubiquitin-ligase Jetlag (JET, **Figure 1a**)[8,19,20]. Recognition of TIM by CRY is hence the molecular event that sensitizes the clock to light. Although light-sensing CRYs have also been developed as powerful tools for optogenetic applications[21,22]; there is little direct structural information on how light-activated CRYs recognize their targets.

CRY:TIM structure determination

To overcome the challenge of isolating sufficient amounts of TIM (1398 residues) for structural characterization by cryo-electron microscopy (cryo-EM), we developed an insect (Drosophila S2) cell-based expression and nanobody-based affinity purification workflow for isolation of the 264 kDa CRY:TIM (**Supplementary Methods Overview**). To produce CRY:TIM, a CRY variant that lacks the 22-residue CCE[23] and therefore binds TIM constitutively[24,25] was co-transfected and expressed in S2 cells with S-TIM. Co-expression with CRYΔ substantially increased TIM levels when ubiquitin-mediated degradation was also chemically blocked (see **Methods**). Nanobody-based affinity resin directed at a 13-residue ALFA tag allowed enrichment and elution of the complex. Complex homogeneity was further improved, and aggregation avoided by crosslinking

with the lysine-specific reagent disuccinimidyl sulfoxide (DSSO) followed by SEC separation (**Extended Data Fig. 1**). Eluted samples were applied directly to glow-discharged Quantifoil® grids, vitrified, and imaged on a 200 keV Talos Arctica microscope equipped with a Gatan Quantum LS energy filter and K3 direct electron camera. Two out of three 3D classes were refined to yield global 3.48 Å (~98 k particles) and 3.3 Å (~160 k particles) maps of the complex **(Extended Data Fig. 1 and Supplementary Table 1**). We built an atomic model based on better resolved TIM density in the 3.3 Å map (**Supplementary Video 1**). Local resolution at the complex interface and within the body exceeds 2.5 Å.

CRY recognizes the TIM N-terminus

The core of TIM revealed in the CRY:TIM complex (residues 1-248; 575-783; and 992-1128, **Figure 1b, Extended Data Fig. 2, and Supplementary Video 1)** forms a continuous right-handed supercoil of armadillo (ARM) 3-helix repeats[26] in which two ARM domains discontinuous in sequence (ARM_1 and ARM_2, **Fig. 1c**) associate by swapping their terminal helices (**Extended Fig. 2**). TIM resembles mammalian TIM (mTIM, see below)[27] but contains an N-terminal extension that binds to CRY **(Figure 1d**). The CRY PHR comprises an N-terminal α/β domain and a C-terminal helical domain that harbors the FAD isoalloxazine ring in a central 4-helix bundle formed by α13-α16 (**Figure 1b,c, Extended Data Fig. 3, and Supplementary Video 1**)[28-30]. N-terminal to the bundle, helices α8-α11 compose the top of the flavin binding pocket and interact with the FAD phosphate groups and adenosine moiety (**Extended Data Fig. 3**). In this cofactor-capping region the phosphate binding loop (residues 249-263) following α8 and the protrusion motif (residues 288-306) following α10, distinguish CRYs from PLs (**Figure 1c**)[28]. The phosphate-binding loop, the protrusion motif, and the Ser-rich C-terminal lid (residues 420-446) together comprise the C-terminal coupled motif (CCM, **Figure 1c and Extended Data Fig. 3**) that changes proteolytic sensitivity when CRY becomes light activated[13].

TIM forms a discontinuous interface with CRY both at the N-terminus and C-terminus (**Figures 1b-e**). The principal CRY:TIM interface buries ~1862 $Å^2$ (49 residues) and 1807 $Å^2$ (52 residues) of solvent accessible surface area on TIM and CRY, respectively. TIM primarily binds to CRY through the first three helices of the N-terminal ARM domain (**Figure 1d,e**). ARM_1-α1 binds across CRY α17 and inserts directly into the flavin binding pocket replacing the CRY C-terminal tail (**Figures 1d, 2a, and Extended Data Fig. 4a)**. The contact is dominated by TIM ARM_1-α1-3, ARM_1-α7 and the ARM_1-α9-10 loop which mesh against the CRY CCM (**Figure 1e and Extended**

Data Figs. 2 and 4). At the center of the interface, Met1 and Asp2 extend out from α1 with Met1 packing against the Trp4 indole and embedding among several elements: Tyr250 and Leu251 of the CRY phosphate binding loop, Gly310 on α11, and Tyr158-Gln159 on the α5-α6 loop that extends down from the CRY α/β domain (**Extended Data Figs. 3 and 5**). TIM Leu4 and Leu5 insert deep into the pocket adjacent to CRY Trp314 and the FAD adenine moiety. TIM ARM_1-α2 contacts the CRY C-terminal lid and ARM_1-α7 contacts the CRY protrusion motif, wherein the α10 helix lengthens to project the tip region toward the Met-rich ARM_1-α9-α10 loop at the interface periphery (**Extended Data Figs. 4c,d**).

CRY:TIM implications for photoadaptation

The recognition of TIM ARM_1-α1 by CRY (**Figure 1d**) may explain an evolutionary adaptation in light-sensing by flies. A *Drosophila melanogaster tim* allele (*ls-tim*) causes differential expression of two isoforms; S-TIM, which begins at the N-terminal Met residue found in the structure, and L-TIM, which extends by an additional 23 N-terminal residues owing to introduction of an alternative translational start site (**Figure 1b**)[6,7]. The frequency of *ls-tim* correlates with geographical latitude and may confer a beneficial preference for more robust rhythms and a diapause state of dormancy in climates of more variable light and cooler temperatures. L-TIM reduces interaction with CRY by yeast two-hybrid, has greater stability in fly heads, and diminishes clock responses to light [20,31]. The Met1 amino-terminus projects into a solvent channel at the interface of the two proteins that could therefore accommodate the L-TIM extension (**Figure 1d and Extended Data Fig. 6a**). However, the recognition of S-TIM by CRY through the N-terminal Met residue will be altered by the L-TIM extension (**Figure 1d)**, thereby potentially explaining the capacity of *ls-tim* to alter fly light sensitivity.

A discontinuous TIM binding element

In addition to the principal interaction between TIM ARM_1 and CRY, strong electron density for a TIM helical segment is evident among the C-terminal lid, the C-terminal end of the last CRY PHR helix (α20) and the α5-α6 loop that projects down from the α/β domain (**Figure 1e and Extended Data Fig. 3**). This TIM helix buries 496 $Å^2$ of surface area, interacts with the light-state configuration of the C-terminal lid and binds at the position occupied by the residues that link α20 to the CTT in the dark-state structure, thereby supporting results from interaction studies[25] and providing further evidence that the CTT undocks from the flavin pocket upon light activation[13,15,17].

There are no connections of this density to the ordered TIM ARM core and thus its sequence assignment is provisional; however, after computational modeling of many predicted helical sequence registers, several gave reasonable agreement with the density and stereochemical constraints of the site; however, of these segments only 1209-1219 was also predicted to occupy the site by Alphafold2.1[32] (**Extended Data Fig. 7a**). To further validate binding by the C-terminal disordered region, we performed the SWFTI assay (**Extended Data Fig. 8**) with TIM truncations and the CRY variant H377L that displays constitutive binding to TIM but also retains the CTT[16]. CRY bound TIM 1-1132 and 571-1398 similarly, but with reduced affinity compared to full-length S-TIM. TIM 1133-1398, which contains the proposed peripheral helix, alone bound to CRY-H377L (**Extended Data Fig. 8**). A known mutation of human TIM that removes the analogous region (R1081X) causes familial advanced sleep phase by reducing interactions between mammalian TIM and mCRY2[33]. Thus, although the roles of mCRY and CRY are not the same in animals and insects[2], they may produce similar interactions with the otherwise disordered C-termini of their respective TIM proteins. These interactions may include competition with PER because TIM 1209-1219 associates with CRY in a region that coincides with where mCRY binds the mammalian Period proteins (**Extended Data Fig. 9a**)[34-36].

TIM proteins diverge in function

TIM and mTIM have similar structures in their respective ordered regions (**Extended Data Fig. 9b**), but their functions diverge. In fact, mTIM is more closely related to the Drosophila Timeout protein (TIM-2) than to TIM itself[27,33]. Although mTIM and TIM-2 play some role in circadian rhythms neither are central constituents of the core mammalian oscillator[2]. In contrast, mTIM and its homologs (TOF1 in yeast, SWI1 in and TIM-1 in *C. elegans*) stabilize replication forks during DNA replication, pair sister chromatids and regulate S-phase checkpoints[37]. Tof-1 participates in the large replisome complex in which it binds directly to dsDNA (**Extended Data Fig. 9d**)[38]. TIM and mTIM share a C-terminal domain (PAB) that includes a conserved stretch of the Timeless C region (residues 1051-1096[33]) and binds poly-(ADP-ribose) polymerase – 1 (PARP-1) in mTIM[39]. However, just as the mTIM N-terminus is unsuited to bind mCRY, the TIM PAB is unlikely to bind to PARP-1 because it differs in the interface elements displayed by mTIM (**Extended Data Fig. 9c**). Thus, details of the respective structures indicate that the roles of TIM in the stabilization and co-transport of PER flies are likely distinct from those of mTIM, Tof-1, and TIM-2 in genome maintenance.

158 **Flavin conformational changes**

159 Pronounced changes in the CRY cofactor binding pocket (**Figure 2a**) involve repositioning of the
160 adenosine and ribose moieties, a large switch in the conformation of the diphosphate groups and
161 refolding of the C-terminal lid to interact with TIM ARM_1-α1 and α2. Moreover, the phosphate
162 binding loop collapses into the flavin pocket to allow Asn253, Gln254 and Gln311 to hydrogen
163 bond with the FAD phosphates (**Extended Data Fig. 5a)**. Tyr250 and Leu251 interact with the
164 FAD pocket and make space for the top of TIM ARM_1-α3 to insert Phe58 behind the new
165 conformation of the phosphate-binding loop (**Figure 2b and Extended Data Fig. 5a**). In addition,
166 cofactor-capping helix α8 tilts 20° towards the FAD diphosphates as Arg237 replaces the FAD
167 Mg^{2+} counter ion, for which no electron density is observed (**Figure 2c and Extended Data Fig.**
168 **5b**). The FAD adenine ring slides 1.5 Å relative to the unbound structure, an adjustment
169 compensated by a shift of Phe318 and harboring helix α11 (**Extended Data Fig. 5b**). The 262-
170 to-264 loop also changes structure to accommodate the new diphosphate conformation and
171 Gln311 swivels away from TIM Leu4 (**Extended Data Fig. 5a,c**). The primary light-sensitive
172 reaction of flavin photoreduction and CTT release precedes TIM binding; however, the change in
173 flavin redox state may induce the observed conformational changes of the FAD and serve to
174 restructure CRY for downstream target engagement.

175 The CRY:TIM complex was purified under light. Although the cofactor redox state could not be
176 verified on the cryo-EM grids, CRY light sensitivity studies[15] indicate that the CRY flavin should
177 be photochemically reduced under these conditions. Regardless, TIM likely stabilizes features of
178 the light-state structure. In support of light-activated CRY in the complex, an Asp410-to-Arg381
179 salt bridge critical for flavin binding and the site of the light-insensitive *cryb* mutation[40], appears to
180 break in response to the new conformation of the ribose backbone (**Figure 2c**), in keeping with
181 predictions of light activation from MD simulations[41]. Two conserved histidine residues within the
182 flavin pocket, His377 and His378, participate in the PL catalytic mechanism and are implicated in
183 CTT release and TIM binding[16,18,42]. In the unbound state His378 ND1 hydrogen bonds with O2'
184 of the FAD ribose, but in the TIM complex, His378 tilts away from the ribose hydroxyl to hydrogen
185 bond to the TIM Leu5 carbonyl with NE2 (**Figures 2b,c and Extended Data Fig. 5b**).
186 Substitutions at His378 still allow CTT release, but on/off switching is less robust[16,42]. Protonation
187 of His378 NE2 is likely required for it to interact with the TIM backbone carbonyl and His378
188 protonation may be responsive to the flavin redox state. The H377L substitution substantially
189 increases the binding affinity to TIM in both light and dark[16]. Surprisingly, His377 does not contact

190 TIM directly but rather anchors the restructured phosphate binding loop by hydrogen bonding to
191 the Asn253 carbonyl (**Figure 2c**). CRY flavin reoxidation is reversible, as is redocking of the
192 CTT[13,15,17], which would complete with TIM for the flavin pocket and hence promote CRY release.
193 However, clock resetting does not require complex dissociation because both TIM and CRY are
194 degraded by the ubiquitin-proteosome pathway upon formation of their complex[8,20].

195 **Relationships among CRYs and photolyases**

196 The interaction of CRY with TIM corresponds closely to how 6-4 photolyase recognizes the 6-4
197 crosslinked pyrimidine lesion in damaged DNA (**Figure 3a**). Indeed, TIM α1 residues Leu4 and
198 Leu5 superimpose with the crosslinked base and the TIM polypeptide closely follows the path of
199 5'-to-3' strand-separated DNA (**Figure 3a**)[43]. Key residues in the pocket also share identity and
200 similar positions, with the notable exception of PL Tyr306, which as a Phe in CRY contacts the
201 Leu5 side-chain. TIM and FAD also combine in CRY to mimic interactions of the FBXL3 E3 ligase
202 with apo-mCRYs for their ubiquitin mediated degradation (**Figure 3b**)[44]. E3 ligase recruitment to
203 CRY could only be similar if the flavin is released, which does not occur upon CRY:TIM
204 association. More likely, the E3 ligases recognize structural features unique to the complex.
205 Despite similarities at the primary cofactor pocket, the phosphate binding loop, protrusion motif
206 and C-terminal lid differ in both sequence and conformation among PLs, mCRYs and CRY. CRY
207 also contains a secondary pocket between its two domains that in PLs binds antenna cofactors
208 and in mCRYs mediates contacts with other clock components[9,45]. No cofactors or other
209 constituents are found within the secondary pocket of the CRY:TIM structure; however, it
210 composes a deep cleft typical of a recognition motif (**Extended Data Fig. 6b**).

211 **Regulation of TIM nuclear entry**

212 The TIM structure provides insight into the gating of TIM:PER nuclear entry by the interaction
213 between TIM and importin-α1 (IMPα1). TIM is homologous to the β-catenins, their related family
214 members (HMP-2, p120, plakoglobin, plakophilin, and SYS-1) as well as the importin-α/β
215 karyopherins involved in nuclear transport[5,26,46]. These ARM proteins conserve a positively
216 charged groove on the concave side of their super-helical crescents where they bind extended
217 peptide chains, such as nuclear localization signals (**Figure 4a,b and Extended Data Fig. 10**)[47,48].
218 Two mutations known to block nuclear entry by reducing interactions between TIM and importin-
219 α1 (Thr90Ala and Pro92Leu; S-TIM numbering)[5] localize within the TIM groove (**Figure 4b**) but
220 do not interact with the TIM nuclear localization sequence, which rather extends in a helix along

221 the convex side of the protein (**Figure 4c**). An extended polypeptide with α-helical character
222 binds into the TIM groove adjacent to catenin-conserved Arg (84, 165) and Asn (88, 166) residues
223 (**Extended Data Fig. 10**), and Thr90/Pro92 (**Figure 4b**). Crosslinking mass spectrometry
224 revealed that TIM Lys313 and Lys328 in the disordered TIM domain (249-545) react with Lys
225 residues in the groove and toward the bottom of the crescent (**Figure 4c and Extended Data Fig.**
226 **10**), whereas Lys residues in other disordered regions (400-544; 784-991; 1129-1398) show little
227 crosslinking to TIM or CRY. After extensive modeling, the sequence Ser283-Thr303 was
228 provisionally assigned as the most reasonable fit to the polypeptide density (**Extended Data Fig.**
229 **7b**). This assignment places Asp287 and Asn291 adjacent to the conserved Asn/Arg residues
230 and occludes the Thr90 and Pro92 residues involved in importin-α1 binding (**Figure 4b**).
231
232 Phosphorylation of the TIM-ST stretch of SGG and CK2 phosphorylation sites (SGG: S274, T278;
233 CK2: T282, S286, S290; **Figures 1b and 4b**) increases nuclear entry rates of TIM in pacemaker
234 neurons (s-LVs)[4]. The Ser283-Thr303 polypeptide bound within the TIM groove contains Ser286
235 and Ser290, which belong to this region of regulatory sites[4]. Thus, the structure suggests that
236 phosphorylation at these sites displaces TIM-ST from the groove to expose the Thr90-Pro92
237 recognition motif for importin-α1 and thereby initiate nuclear import (**Figure 4d**). Thus, key delays
238 that tune the clock period through nuclear entry likely depend on the interactions of a TIM
239 autoinhibitory segment that alter upon its timed phosphorylation by circadian kinases.
240
241 The CRY:TIM structure reveals how a light-sensing cryptochrome engages its target. It also
242 provides insight into how evolutionary relationships among the component proteins comprise
243 regulatory circuits. Swapping the auxiliary CTT of CRY for the variable TIM N-terminus not only
244 sets the circadian oscillator but also tunes its light sensitivity. In this interaction, the ability of TIM
245 to serve as a peptide mimetic for a PL DNA substrate underscores how conserved structural
246 features of PLs are also utilized by CRYs. In gating its partnership with CRY, TIM shares an
247 autoinhibitory mechanism that resembles that which regulates importin-α[48-50]. The striking
248 changes in FAD geometry that couple to CRY conformational rearrangement and TIM binding
249 were unexpected. These new insights raise questions as to whether other flavoprotein light-
250 sensors share similar mechanisms to convey light or redox signals from their cofactors.
251

252 ## References
253

1 Takahashi, J. S. Transcriptional architecture of the mammalian circadian clock. *Nature Reviews Genetics* **18**, 164-179 (2017).

2 Crane, B. R. & Young, M. W. Interactive Features of Proteins Composing Eukaryotic Circadian Clocks. *Ann. Rev. Biochem.* **83** (2014).

3 Foley, L. E. & Emery, P. Drosophila Cryptochrome: Variations in Blue. *Journal of Biological Rhythms* **35**, 16-27 (2020).

4 Top, D., Harms, E., Syed, S., Adams, E. L. & Saez, L. GSK-3 and CK2 Kinases Converge on Timeless to Regulate the Master Clock. *Cell Reports* **16**, 357-367 (2016).

5 Jang, A. R., Moravcevic, K., Saez, L., Young, M. W. & Sehgal, A. Drosophila TIM Binds Importin alpha 1, and Acts as an Adapter to Transport PER to the Nucleus. *Plos Genetics* **11** (2015).

6 Tauber, E. *et al.* Natural selection favors a newly derived timeless allele in Drosophila melanogaster. *Science* **316**, 1895-1898 (2007).

7 Deppisch, P. *et al.* Adaptation of Drosophila melanogaster to Long Photoperiods of High-Latitude Summers Is Facilitated by the ls-Timeless Allele. *J. Biol. Rhythms* **37**, 185-201 (2022).

8 Lin, F. J., Song, W., Meyer-Bernstein, E., Naidoo, N. & Sehgal, A. Photic signaling by cryptochrome in the Drosophila circadian system. *Molecular and Cellular Biology* **21**, 7287-7294 (2001).

9 Chaves, I. *et al.* The cryptochromes: blue light photoreceptors in plants and animals. *Annual review of plant biology* **62**, 335-364 (2011).

10 Ozturk, N. Phylogenetic and Functional Classification of the Photolyase/Cryptochrome Family. *Photochemistry and Photobiology* **93**, 104-111 (2017).

11 Parico, G. C. G. *et al.* The human CRY1 tail controls circadian timing by regulating its association with CLOCK:BMAL1. *Proceedings of the National Academy of Sciences of the United States of America* **117**, 27971-27979 (2020).

12 Berndt, A. *et al.* A novel photoreaction mechanism for the circadian blue light photoreceptor Drosophila cryptochrome. *J Biol Chem* **282**, 13011-13021 (2007).

13 Vaidya, A. T. *et al.* Flavin reduction activates Drosophila cryptochrome. *Proc Natl Acad Sci U S A* **110**, 20455-20460 (2013).

14 Ozturk, N., Selby, C.P., Annayev, Y., Zhong, D., Sancar, A. Reaction Mechanism of Drosopila cryptochrome. *Proc Natl Acad Sci U S A* **108**, 516-521 (2011).

15 Lin, C. F., Top, D., Manahan, C. C., Young, M. W. & Crane, B. R. Circadian clock activity of cryptochrome relies on tryptophan-mediated photoreduction. *Proceedings of the National Academy of Sciences of the United States of America* **115**, 3822-3827 (2018).

16 Lin, C., Schneps, C. M., Chandrasekaran, S., Ganguly, A. & Crane, B. R. Mechanistic insight into light-dependent recognition of Timeless by Drosophila Cryptochrome. *Structure* (2022).

17 Chandrasekaran, S. *et al.* Tuning flavin environment to detect and control light-induced conformational switching in Drosophila cryptochrome. *Communications biology* **4**, 1-12 (2021).

18 Ganguly, A. *et al.* Changes in active site histidine hydrogen bonding trigger cryptochrome activation. *Proceedings of the National Academy of Sciences of the United States of America* **113**, 10073-10078 (2016).

19 Koh, K., Zheng, X. Z. & Sehgal, A. JETLAG resets the Drosophila circadian clock by promoting light-induced degradation of TIMELESS. *Science* **312**, 1809-1812 (2006).

20 Peschel, N., Chen, K. F., Szabo, G. & Stanewsky, R. Light-Dependent Interactions between the Drosophila Circadian Clock Factors Cryptochrome, Jetlag, and Timeless. *Current Biology* **19**, 241-247 (2009).

21 Yu, D. *et al.* Optogenetic activation of intracellular antibodies for direct modulation of endogenous proteins. *Nat Methods* **16**, 1095-1100 (2019).

22 Gil, A. A. *et al.* Optogenetic control of protein binding using light-switchable nanobodies. *Nat Commun* **11**, 4044 (2020).

23 Busza, A., Emery-Le, M., Rosbash, M. & Emery, P. Roles of the two Drosophila CRYPTOCHROME structural domains in circadian photoreception. *Science* **304**, 1503-1506 (2004).

24 Dissel, S. *et al.* A constitutively active cryptochrome in Drosophila melanogaster. *Nat. Neurosci.* **7**, 834-840 (2004).

25 Hemsley, M. J. *et al.* Linear motifs in the C-terminus of D-melanogaster cryptochrome. *Biochemical and Biophysical Research Communications* **355**, 531-537 (2007).

26 Vodovar, N., Clayton, J. D., Costa, R., Odell, M. & Kyriacou, C. P. The Drosophila clock protein Timeless is a member of the Arm/HEAT family. *Current Biology* **12**, R610-R611 (2002).

27 Holzer, S. *et al.* Crystal structure of the N-terminal domain of human Timeless and its interaction with Tipin. *Nucleic Acids Research* **45**, 5555-5563 (2017).

28 Zoltowski, B. D. *et al.* Structure of full-length Drosophila cryptochrome. *Nature* **480**, 396-399 (2011).

29 Levy, C. *et al.* Updated structure of Drosophila cryptochrome. *Nature* **495**, E3-4 (2013).

30 Czarna, A. *et al.* Structures of Drosophila cryptochrome and mouse cryptochrome1 provide insight into circadian function. *Cell* **153**, 1394-1405 (2013).

31 Sandrelli, F. *et al.* A molecular basis for natural selection at the timeless locus in Drosophila melanogaster. *Science* **316**, 1898-1900 (2007).

32 Jumper, J. *et al.* Highly accurate protein structure prediction with AlphaFold. *Nature* **596**, 583-589 (2021).

33 Kurien, P. *et al.* TIMELESS mutation alters phase responsiveness and causes advanced sleep phase. *Proceedings of the National Academy of Sciences of the United States of America* **116**, 12045-12053 (2019).

34 Schmalen, I. *et al.* Interaction of Circadian Clock Proteins CRY1 and PER2 Is Modulated by Zinc Binding and Disulfide Bond Formation. *Cell* **157**, 1203-1215 (2014).

35 Fribourgh, J. L. *et al.* Dynamics at the serine loop underlie differential affinity of cryptochromes for CLOCK:BMAL1 to control circadian timing. *Elife* **9** (2020).

36 Nangle, S. N. *et al.* Molecular Assembly of the Period-Cryptochrome Circadian Transcriptional Repressor Complex. *Elife* **3** (2014).

37 Engelen, E. *et al.* Mammalian TIMELESS Is Involved in Period Determination and DNA Damage-Dependent Phase Advancing of the Circadian Clock. *PLoS One* **8** (2013).

38 Baretic, D. *et al.* Cryo-EM Structure of the Fork Protection Complex Bound to CMG at a Replication Fork. *Molecular Cell* **78**, 926-+ (2020).

39 Xie, S. *et al.* Timeless Interacts with PARP-1 to Promote Homologous Recombination Repair. *Molecular Cell* **60**, 163-176 (2015).

40 Stanewsky, R. *et al.* The cry(b) mutation identifies cryptochrome as a circadian photoreceptor in Drosophila. *Cell* **95**, 681-692 (1998).

41 Wang, Y. J., Veglia, G., Zhong, D. P. & Gao, J. L. Activation mechanism of Drosophila cryptochrome through an allosteric switch. *Science Advances* **7** (2021).

42 Berntsson, O. *et al.* Photoactivation of Drosophila melanogaster cryptochrome through sequential conformational transitions. *Science Advances* **5** (2019).

43 Glas, A. F., Schneider, S., Maul, M. J., Hennecke, U. & Carell, T. Crystal Structure of the T(6-4)C Lesion in Complex with a (6-4) DNA Photolyase and Repair of UV-Induced (6-4) and Dewar Photolesions. *Chemistry-a European Journal* **15**, 10387-10396 (2009).

44 Nangle, S., Xing, W. M. & Zheng, N. Crystal structure of mammalian cryptochrome in complex with a small molecule competitor of its ubiquitin ligase. *Cell Research* **23**, 1417-1419 (2013).

45 Rosensweig, C. *et al.* An evolutionary hotspot defines functional differences between CRYPTOCHROMES. *Nature Communications* **9** (2018).

46 Tewari, R., Bailes, E., Bunting, K. A. & Coates, J. C. Armadillo-repeat protein functions: questions for little creatures. *Trends in Cell Biology* **20**, 470-481 (2010).

359 47 Choi, H. J. *et al.* A Conserved Phosphorylation Switch Controls the Interaction between
360 Cadherin and beta-Catenin In Vitro and In Vivo. *Developmental Cell* **33**, 82-93 (2015).

361 48 Goldfarb, D. S., Corbett, A. H., Mason, D. A., Harreman, M. T. & Adam, S. A. Importin
362 alpha: a multipurpose nuclear-transport receptor. *Trends in Cell Biology* **14**, 505-514
363 (2004).

364 49 Catimel, B. *et al.* Biophysical characterization of interactions involving importin-alpha
365 during nuclear import. *Journal of Biological Chemistry* **276**, 34189-34198 (2001).

366 50 Harreman, M. T., Hodel, M. R., Fanara, P., Hodel, A. E. & Corbett, A. H. The auto-
367 inhibitory function of importin alpha is essential in Vivo. *Journal of Biological Chemistry*
368 **278**, 5854-5863 (2003).

369 **Figure Legends**
370

371 **Figure 1. Cryo-EM structure of the CRY:TIM complex.** (**a**) Drosophila Cryptochrome (CRY)
372 entrains the circadian clock by initiating degradation of Timeless (TIM) in light. Jetlag (JET),
373 Period (PER), Doubletime (DB), Cycle (CYC), Clock (CLK) and Importin-α1 (IMPα1) compose the
374 core circadian oscillator. (**b**) CRY:TIM docked into the electron density map. Dark-state CRY
375 shown at the bottom (grey, PDB ID: 4GU5). (**c**) Domain arrangements and key regions of CRY
376 and TIM. Features of TIM: CRY-binding domains (CRY-BD1, 1-234, CRY-BD2, 1133-1398),
377 serine/threonine-rich region (ST, 270-290) with key phosphorylation sites starred (S274, T278,
378 T282, S286 and S290), ARM1 (1-248), ARM2 (578-866), nuclear localization sequence (NLS,
379 545-578), Parp-1 binding domain (PAB, 986-1142; TIM-C, 1051-1096), 23 residue L-TIM
380 extension (L, (23aa)), disordered regions are dashed. Features of CRY: Phosphate binding loop
381 (PL, 249-263), Protrusion motif (PM, 288-306), C-terminal lid (CL, 420-446), C-terminal tail (CTT,
382 519-542, absent in CRYΔ). (**d**) N-terminus of TIM inserts into the primary flavin binding pocket.
383 2.4 Å resolution local electron density is shown with notable hydrogen bonds (yellow dashes) and
384 hydrophobic contacts (green circle). (**e**) Interface between CRY and TIM (blue shaded area), TIM
385 groove peptide (in navy blue) and peripheral helix (fitted with 1209-1219 provisionally, blue). Inset
386 shows the interactions between TIM 1209-1219 and CRY superimposed with electron density.
387

388 **Figure 2. Conformational changes of FAD to the CRY C-terminal coupled motif upon**
389 **binding TIM.** (**a**) CRY:TIM (CRY, yellow; TIM, blue) in superposition with dark-state CRY. The
390 N-terminus of TIM replaces the CRY CTT (red), as depicted in the schematic below. Structural
391 elements designated as in **Figure 1**. A CTT-like sequence on TIM (617-626) that in isolation binds
392 light-state CRY[13] locates in the ARM core remote from the interface and is thus unlikely to be a
393 binding determinant. (**b**) The phosphate binding loop (dark pink) collapses into the flavin pocket

394 and N253 and E254 hydrogen bond (yellow dashes) with the FAD diphosphate conformation (red,
395 orange) that differs substantially from that of the dark state (white bonds). (**c**) R237 replaces the
396 Mg^{2+} counter ion and H377 anchors the new position of the loop. The D410-R381 salt bridge (top)
397 appears to break in response to the new conformation of the ribose backbone (bottom). Reduced
398 side-chain density of R381 suggests increased flexibility in the TIM complex.
399
400 **Figure 3. Conservation of recognition modes by CRY family members.** (**a**) The interaction of
401 CRY with TIM corresponds closely to how 6-4 photolyase recognizes the 6-4 pyrimidine lesion in
402 damaged DNA (PDB ID:3CVU). TIM Leu4 and Leu5 superimpose on the crosslinked bases and
403 the TIM ARM1- α1 polypeptide closely follows the path of 5'-to-3' strand-separated DNA. (**b**) The
404 TIM and FAD contacts of CRY mimic the interaction of apo-mCRY with the C-terminus of the
405 FBXL3 E3 ligase (PDB ID: 4I6J).
406
407 **Figure 4. A structural basis for regulation of TIM nuclear entry.** (**a**) Electron density (dark
408 blue) for an extended polypeptide resides within a groove wherein members of the β-catenin and
409 α-importin proteins bind their target sequences. (**b**) The TIM groove peptide density shown with
410 the sequence assignment S283-T303. The peptide interacts with β-catenin-conserved Asn and
411 Arg residues and buries residues important for importin-α1 binding (T90 and P92). (**c**) DSSO-
412 mediated lysine crosslinking patterns of disordered residues K313 and K238 shown on the TIM
413 structure. K313 and K328 produce a pattern of crosslinking that localizes them to a position
414 consistent with placement of the S283-T303 groove peptide. The TIM NLS lies in a helix adjacent
415 to the groove but does not occlude T90 and P92. (**d**) Schematic of proposed nuclear entry
416 mechanism of TIM. Phosphorylation of the TIM-ST region by SGG and CK2 releases the ST
417 region from TIM groove to expose TIM T90 and P92. Importin-α1 binds TIM adjacent to Thr90
418 and Pro92, while also binding the TIM NLS within a structurally analogous ARM groove of its own.
419
420 ## Methods
421 ### Cloning
422 All DNA constructs (given in the Supplementary Information) were built by a modified Gibson
423 assembly method and Q5 polymerase-based mutagenesis with home-made reaction mixture, as
424 reported previously[51].
425
426 ### Transient co-transfection of S2 cells

427 S2 cells (cat# CRL-1963, ATCC) were maintained at 27 °C in 90% Schneider's Drosophila
428 Medium (Cat# 21720024, ThermoFisher) suppled with 10% heat-inactivated Fetal Bovine Serum
429 (FBS, Cat# F4135, sigma), as reported previously[51]. pAC5.1 vectors of CLIP-CRYΔ and TIM-
430 SNAP-HA-ALFA were delivered into S2 cells using the TransIT-Insect Transfection Reagent
431 (Cat# MIR6100, Mirus) following a modified version of the manufacturer's instruction. Briefly,
432 about twenty 100 mm culture dishes (Cat# 353003, Corning) with 1000×10^4 cells in 10 ml fresh
433 growth medium were prepared on day 1. About 20 hours later, 10 µg DNA in total (CRYΔ: TIM
434 mass ratio 1:1) were transfected by the TransIT-Insect reagent in each 100 mm dish. 72 hours
435 after transfection, cells were harvested by centrifugation with 500 × g for 5 minutes at room
436 temperature, washed once with chilled PBS and then stored at -80 °C until lysis.
437
438 **Nanobody-based affinity purification of the CRY:TIM complex**
439 Two cycles of freeze-thaw were used to lyse the S2 cells as follows: S2 cell pellets from 200 ml
440 of culture were resuspended with 16 ml lysis buffer (50 mM Tris, pH 8, NaCl 150 mM, 20% glycerol,
441 1x protease inhibitor (Cat# A32965, ThermoFisher)), divided as 800 µL aliquots in each tube and
442 flash frozen in liquid nitrogen. The 800 µl aliquots were then quickly thawed in a room temperature
443 water bath. The lysate aliquots were resupended (without vortexing) and the freeze-thaw cycle
444 repeated. 100 U/ml benzonase (sc-202391, Santa Cruz Biotechnology) was added to the sample
445 and incubated at 4 °C for 45 min to remove DNA/RNA contamination. The cell lysate was spun at
446 20000 x g for 20 minutes at 4 °C and further filtered with a 0.45 micron PVDF syringe filter (Cat#
447 SLHV033NB, Millipore Sigma). 320 µL of ALFA resin 50% slurry (cat# N1512, Nanotag
448 Biotechnologies) was equilibrated with lysis buffer and then incubated with the cell lysate at 4 °C
449 for 1 h on an end-to-end rotator (Cat# 88881001, ThermoFisher scientific). The slurry was
450 transferred to a 15 ml falcon tube, centrifuged at 1000 x g for 1 min and wash the resin with 7 mL
451 wash buffer (HEPES 50 mM, pH 7.9, NaCl 150 mM, 10% glycerol). This process was repeated 3
452 times. Then the resin was resuspended in 1 mL wash buffer and split into two and applied to
453 separate spin columns (Cat# 6572, BioVision), with 80 µL resin applied to each column. The spin
454 columns were washed 4 times with 500 µl wash buffer and spun down at 1000 x g. 80 µL resin in
455 each spin column was resuspended in 500 µL elution buffer (wash
456 buffer with 200 µM ALFA peptide, cat# N1520, Nanotag Biotechnologies) and incubated in the
457 cold room for 20 min on an end-to-end rotator. The columns were spun at 1000 x g for 1 min to
458 collect the elution. The elution was repeated 3 times and all of the elution samples were then
459 combined (3 mL in total).
460

461 **DSSO crosslinking coupled with SEC**

462 The elution was concentrated to about 70 to 80 μL (while maintaining the final protein
463 concentration at less than 2 mg/mL to ensure efficient crosslinking) with a 30 kDa vivaspin
464 concentrator (Cat# 28932235, Cytiva). 50 mM stock solution of DSSO (cat# A33545,507
465 ThermoFisher or cat# 9002863, Cayman Chemicals) was prepared in dimethyl sulfoxide (DMSO).
466 DSSO was added to the elution sample to a final concentration of 1 mM and incubated at room
467 temperature for 45 minutes, followed by quenching for 5 min at room temperature with addition of
468 1 M Tris buffer (pH 8) to produce a final concentration of 20 mM Tris. The crosslinked complex
469 was concentrated by 50 kDa vivaspin (Cat# 28932236, Cytiva) and purified by a Superose SEC
470 column 6 10/300 (Cat# 29091596, Cytiva) or 3.2/300 (Cat# 29091598, Cytiva). The protein
471 complex was eluted in SEC buffer (20 mM HEPES, pH 7.9, 150 mM NaCl) and concentrated to
472 ~40 μL by a 50 kDa cutoff vivaspin concentrator.

473

474 **Cross-Linking Mass Spectrometry (XL-MS)**

475 SEC-purified crosslinked product was mixed with 4x Laemmli Sample Buffer (Cat# 1610747,
476 BioRad) and 2.5% 2-mercaptoethanol (BME, Cat# 1610710, BioRad) and then boiled for 6 min.
477 The sample was then loaded on an SDS-PAGE gel and stained with QC Colloidal Coomassie
478 Stain (Cat #1610803, BioRad). The band of the complex (~ 20 ug protein sample) was cut out
479 and prepared for MS-MS analysis of crosslinked peptides as previously reported[52] and described
480 below.

481

482 **In-gel digestion of SDS gel bands**

483 The protein band (~ 20 µg protein) was sliced into ~1 mm cubes. The excised gel pieces were
484 washed consecutively with 400 µL deionized water followed by 50 mM ammonium bicarbonate,
485 50% acetonitrile and finally 100% acetonitrile. The dehydrated gel pieces were reduced with 200
486 µL of 10 mM DTT in 100 mM ammonium bicarbonate for 45 min at 56 °C, followed by alkylation
487 with 200 µL of 55 mM iodoacetamide in 100 mM ammonium bicarbonate at room temperature in
488 the dark for 45 min. Wash steps were repeated as described above. The gel was then dried and
489 rehydrated with 100 µL LysC at 10 ng/µL in 50 mM ammonium bicarbonate containing 10%
490 acetonitrile (ACN) and incubated at 37 °C for 3 h. After the 3 h incubation, 30 µL Trypsin at 43
491 ug/uL in 50 mM ammonium bicarbonate was added and the sample was continued to incubate at
492 37 °C for 18 h. The digested peptides were extracted from the gel twice with 200 µL of 50%
493 acetonitrile containing 5% formic acid and once with 200 µL of 75% acetonitrile containing 5%
494 formic acid. Extractions from each sample were pooled together and then divided equally in half.

495 One half was then filtered with 0.22 µm spin filter (Costar Spin-X from Corning), dried to dryness
496 in the speed vacuum and analyzed as LysC/Trypsin digests. The second half was dried to
497 dryness in the speed vacuum then reconstituted with 30 µL GluC at 33 ng/µL in 50mM ammonium
498 bicarbonate (pH 7.9), incubated at 37 °C for 18 h. After incubation, formic acid was added to stop
499 enzyme reaction. The digests were filtered with 0.22 µm spin filter, dried to dryness in the speed
500 vacuum and analyzed as LysC/Trypsin/GluC digests. Each sample was reconstituted in 0.5%
501 formic acid prior to LC- MS/MS analysis.
502
503 **Crosslinks identification by nanoLC-MS/MS**
504 The digested product was characterized by NanoLC-MS/MS analysis at the Cornell Biotechnology
505 Resource Center. The analysis was carried out using an Orbitrap Fusion™ Tribrid™ (Thermo-
506 Fisher Scientific, San Jose, CA) mass spectrometer equipped with a nanospray Flex Ion Source,
507 and coupled with a Dionex UltiMate 3000 RSLCnano system (Thermo, Sunnyvale, CA). Each
508 sample was loaded onto a nano Viper PepMap C18 trapping column (5 µm, 100 µm × 20 mm,
509 100 Å, Thermo Fisher Scientific) at 20 µL/min flow rate for rapid sample loading. After 3 minutes,
510 the valve switched to allow peptides to be separated on an Acclaim PepMap C18 nano column
511 (2 µm, 75 µm x 25 cm, Thermo Fisher Scientific) at 35 °C in a 90 min gradient of 5% to 40% buffer
512 B (98% ACN with 0.1% formic acid) at 300 nL/min. The Orbitrap Fusion was operated in positive
513 ion mode with nano spray voltage set at 1.7 kV and source temperature at 275 °C. External
514 calibrations for Fourier transform, ion-trap and quadrupole mass analyzers were performed prior
515 to the analysis. Samples were analyzed using the CID-MS^2-MS^3 workflow, in which MS scan
516 range was set to 375–1500 m/z and the resolution was set to 60,000. Precursor ions with charge
517 states 3-8 were selected for CID MS^2 acquisitions in Orbitrap analyzer with a resolution of 30,000
518 and an AGC target of 5×10^4. The precursor isolation width was 1.6 m/z and the maximum
519 injection time was 100 ms. The CID MS^2 normalized collision energy was set to 25%. Targeted
520 mass-difference triggered HCD-MS^3 spectra were acquired in the ion trap with AGC target of 1
521 $\times 10^4$. When a unique mass difference (Δ=31.9721 Da) was observed in CID-MS^2 spectra for ions
522 with a single charge and multiple charges, the HCD collision energy at 38% and 28% was used
523 respectively, for the subsequent MS^3 scans. All data were acquired under Xcalibur 4.3 operation
524 software and Orbitrap Fusion Tune application v3.4 (Thermo-Fisher Scientific).
525
526 **MS Data analysis**
527 All MS, MS^2 and MS^3 raw spectra from each sample were searched using Proteome Discoverer
528 2.4 (Thermo-Fisher Scientific, San Jose, CA) with XlinkX v2.0 algorithm for identification of

529 crosslinked peptides. The search parameters were as follow: four missed cleavage for either
530 double digestion or triple digestion with fixed carbamidomethyl modification of cysteine, variable
531 modifications of methionine oxidation, asparagine and glutamine deamidation, protein N-terminal
532 acetylation. The peptide mass tolerance was 10 ppm, and MS^2 and MS^3 fragment mass tolerance
533 was 20 ppm and 0.6 Da, respectively. The *Drosophila melanogaster* database with added
534 targeted protein sequences was used for PD 2.4 database search with 1% FDR for report of
535 crosslink results. Identified crosslinked peptides were filtered for Max. XlinkX Score > 40
536 containing at least two identified MS^3 spectra for each pair of crosslinked peptides. Search Results
537 were exported by the software as a spreadsheet. The crosslinked peptides were analyzed by
538 xiNET for generating the viewer of inter or inner crosslinks between two target proteins.
539
540 **SWFTI assay**
541 S2 cells were co-transfected as described above with pAC 5.1 vectors of CLIP-CRY-377L and
542 TIM-SNAP-HA-ALFA variants at a mass ratio of 3:1. The pulldown assay was carried out as
543 follows, similar to that previously described[51]. 5 mL of S2 cell pellets were lysed with 400 µL lysis
544 buffer containing non-ionic detergent (50 mM Tris buffer, pH 8, 150 mM NaCl, 1% IGEPAL CA-
545 630 (Cat# I8896, Sigma Aldrich), 10% glycerol and 1x protease inhibitor (Cat# A32965,
546 ThermoFisher)) was added to cell pellets harvested from 5 mL cells. EDTA was omitted to avoid
547 disturbing SNAP/CLIP dye labeling. All buffer pHs were adjusted at the working temperature. After
548 cells were incubated with lysis buffer on ice for 30 mins (flicking the tube every 10 min to avoid
549 vortexing), cell debris was removed by spinning at 15,000 × g for 15 minutes at 4°C.
550 To label the lysate sample with SNAP/CLIP dyes, 1 part of lysate was diluted with 2 parts of
551 labeling buffer (50 mM Tris buffer, pH 8, 150 mM NaCl, 10% glycerol) to decrease the
552 concentration of non-ionic detergent to less than 0.5%, as recommended by the manufacturer
553 (New England Biolabs). Then 27 µL of diluted lysate was mixed with 1 µL of 0.1 mM SNAP dye
554 (Cat# S9102S, SNAP-Cell 647-SiR), 1 ul 0.1 mM CLIP dye (Cat# S9217S, CLIP-Cell 505) and 1
555 ul 30 mM DTT and incubated in the dark at room temperature for 1 hour. 10 uL 4x Laemmli sample
556 buffer (Cat# 1610747, BioRad) and 1.5 µL 2-mercaptoethanol (BME) was added to the 30 µL mix,
557 boiled at 95 °C for 5 minutes. After labeling with the SNAP/CLIP substrate, the sample was
558 protected from bright light to avoid photobleaching. 20 µL of the sample was loaded on a gradient
559 stain-free gel (Cat# 4568095, BioRad) to perform SDS-PAGE. The result was imaged with
560 Chemidoc (BioRad) and quantified by image lab software (BioRad).
561

562 To label CRY and TIM on the affinity resin, ~350 µL cell lysate was mixed with 10 µL pre-washed
563 magnetic HA resin slurry (Cat# 88836, ThermoFisher) and incubated on an end-to-end rotator
564 overnight at 4 °C. The dark sample was covered by foil and kept in the dark. Next day, the resin
565 was washed with room temperature 500 µL TBS-T (20 mM Tris buffer, pH 7.6, 150 mM NaCl,
566 0.05% Tween-20) four times. Then HA resin was resuspended in 27 µL labeling buffer, 1 µL 0.1
567 mM SNAP dye, 1 µL 0.1 mM CLIP dye and 1 µL 30 mM DTT. The tube was incubated in the dark
568 on an end-to-end rotator at room temperature for one hour. Subsequently, 10 µL 4x Laemelli
569 sample buffer and 1.5 µL BME were added to the 30 µL resin mix. The tube was boiled at 95 °C
570 for 10 minutes to denature and elute CRY and TIM from HA resin. SDS-PAGE and imaging were
571 performed the same as above. Effective KD values were calculated as described elsewhere[51].
572
573 **Negative Stain Electron Microscopy**
574 Initial CRY:TIM samples were screened by negative-stain. Formvar/carbon 200 mesh copper
575 grids (Electron Microscopy Sciences) was plasma cleaned by the GloQube glow discharge
576 system (Electron Microscopy Sciences). Ten µL of 0.05 mg/ml CRY:TIM solution was applied
577 onto the grid, incubated for 30 seconds, and the excess solution was blotted with filter paper. 10
578 µl of 2% uranyl acetate was then applied to the grid twice for 30-second incubation followed by
579 blotting. The grid was air-dried for 5 minutes and visualized by Philips Morgagni 268 Transmission
580 Electron Microscope at 100 keV.
581
582 **Cryo-EM grid preparation and data collection of CRY:TIM complex**
583 Four µL of 0.5 mg/ml CRY:TIM solution was applied to glow-discharged grids (300 mesh
584 Quantifoil Au, R1.2/1.3) that were purchased from Electron Microscopy Sciences. After 30
585 seconds incubation, the excess solution was blotted for 4 sec with filter paper by a Vitrobot Mark
586 IV (Thermo Fischer Scientific). Grids were subsequently vitrified in liquid ethane and stored in
587 liquid nitrogen. Cryo-EM images of CRY:TIM complex were collected on a Talos Arctica (Thermo
588 Fischer Scientific) operated at 200 keV at a nominal magnification of 79,000x with Gatan GIF
589 Quantum LS Imaging energy filter, using a Gatan K3 direct electron camera in counting mode,
590 corresponding to a pixel size of 0.516 Å. A total of 1636 images stacks were obtained with a
591 defocus rage of -0.8 to -2.0 µm by EPU (Thermo Fischer Scientific). Each stack movie was
592 recorded for a total dose of 53 e-/Å^2.
593
594 **Cryo-EM data processing of the CRY:TIM complex**

595 Dose fractionated image stacks were subjected to motioncor2[53] wrapped in Relion 3.1.3 [54]
596 followed by patch CTF estimation in CryoSparc v3.2.0[55]. The micrographs whose CTF estimation
597 is greater than 4 Å were chose for later processing, which yielded 1473 micrographs. Blob picker
598 in CryoSparc was used on the three hundred randomly selected micrographs, which was followed
599 by 2D classification and generation of ~23k particles for the first-round Topaz train[56]. Then the
600 trained model was applied to all 1473 micrographs and ~48k particles were extracted and selected
601 by 2D classification for the second-round of Topaz train particle identification. After two rounds of
602 Topaz train and extraction, in totality ~2M particles were picked. Following 2D classification non-
603 relevant particles were removed and only the best classes were kept (~350k particles). The
604 particle stack was subjected to Bayesian polishing in RELION 3.1.3 and imported back to
605 CryoSparc for the further Ab Initio reconstruction and Heterogenous refinement with 3 classes.
606 The second and third classes were selected, and multiple rounds of Homogenous and Non-
607 uniform Refinement were performed to yield a global 3.48 Å (~98k particles) and a global 3.3 Å
608 (~160k particles) map using "gold standard" FSC at 0.143 cut-off, respectively. The 3.3 Å map is
609 subjected to the model building. C1 symmetry was used throughout data processing. The
610 workflow is provided in Extended Figure 1.
611
612 **Model building and refinement of the CRY:TIM complex**
613 The initial CRY model is adapted from the PDB entry 4GU5, and the initial TIM model was fetched
614 from AlphaFold Protein Structure Database entry P49021[57]. Both models were manually docked
615 into the map by UCSF ChimeraX[58]. The model was subjected to ISOLDE[59] to fit the loops which
616 undergo conformational changes into the map density. Intrinsically disordered loops of TIM which
617 were not visualized in the map were not included in the model. The CRY:TIM model was subjected
618 to multiple rounds of automatic refinement using Phenix real space refinement, and manually
619 building using Coot[60-62]. Validation was performed by MolProbity[63]. The final refinement statistics
620 is provided in Table S1.
621
622 The unassigned polypeptide in the TIM grove was built in both directions and the sequence
623 register slid along the backbone for a 150 residue stretch in the 250-400 range and each register
624 real-spaced refined against the electron density and Q-score[64] calculated. Given the helical nature
625 of the density at one end of the groove, directionality of the sequence was best fit with the
626 polypeptide having its N-terminal end closest to CRY and the C-terminal end running toward the
627 Lys313/328 crosslinking partners at the base of the groove. Side chain density in the helical region
628 showed a variable size pattern that was inconsistent with the repetitive patterns of much of the

disordered region beyond residue 350. C-terminal to the groove peptide Lys313 and Lys328 are unresolved, but should be closely positioned to their crosslinking partners. To assign sequence to the disconnected TIM helix binding the PHR C-terminus secondary structure predictions on the regions of TIM not resolved in the ordered core were performed by RAPTORX[65]. All predicted helical sequences were fit into the density and refined in real-space with a range of sequence registers. As an additional check AlphaFold2.1[57] was used to predict interactions between CRY and the disordered region of TIM, with the highest scoring predictions also tested for agreement with the electron density map. The disconnected helix displays strong side-chain density, which sets its directionality and ruled out many sequence placements. Given the resolution limitations of the cryo-EM maps, we consider the sequence assignments of both of these helical regions tentative.

Analysis of TIM structural homologs

Structural comparisons and sequence alignments of TIM structural homologs were carried out with the DALI server[66].

Methods References

51 Lin, C., Schneps, C. M., Chandrasekaran, S., Ganguly, A. & Crane, B. R. Mechanistic insight into light-dependent recognition of Timeless by Drosophila Cryptochrome. *Structure* (2022).

52 Muok, A. R. *et al.* Engineered chemotaxis core signaling units indicate a constrained kinase-off state. *Science Signaling* **13** (2020).

53 Zheng, S. Q. *et al.* MotionCor2: anisotropic correction of beam-induced motion for improved cryo-electron microscopy. *Nat Methods* **14**, 331-332 (2017).

54 Scheres, S. H. RELION: implementation of a Bayesian approach to cryo-EM structure determination. *J Struct Biol* **180**, 519-530 (2012).

55 Punjani, A., Rubinstein, J. L., Fleet, D. J. & Brubaker, M. A. cryoSPARC: algorithms for rapid unsupervised cryo-EM structure determination. *Nat Methods* **14**, 290-296 (2017).

56 Bepler, T. *et al.* Positive-unlabeled convolutional neural networks for particle picking in cryo-electron micrographs. *Nat Methods* **16**, 1153-1160 (2019).

57 Jumper, J. *et al.* Highly accurate protein structure prediction with AlphaFold. *Nature* **596**, 583-589 (2021).

58 Pettersen, E. F. *et al.* UCSF ChimeraX: Structure visualization for researchers, educators, and developers. *Protein Sci* **30**, 70-82 (2021).

59 Croll, T. I. ISOLDE: a physically realistic environment for model building into low-resolution electron-density maps. *Acta Crystallogr D Struct Biol* **74**, 519-530 (2018).

60 Morin, A. *et al.* Collaboration gets the most out of software. *Elife* **2**, e01456 (2013).

61 Emsley, P., Lohkamp, B., Scott, W. G. & Cowtan, K. Features and development of Coot. *Acta Crystallogr D Biol Crystallogr* **66**, 486-501 (2010).

62 Liebschner, D. *et al.* Macromolecular structure determination using X-rays, neutrons and electrons: recent developments in Phenix. *Acta Crystallogr D Struct Biol* **75**, 861-877 (2019).

63 Chen, V. B. *et al.* MolProbity: all-atom structure validation for macromolecular crystallography. *Acta Crystallogr D Biol Crystallogr* **66**, 12-21 (2010).

64 Pintilie, G. *et al.* Measurement of atom resolvability in cryo-EM maps with Q-scores. *Nat Methods* **17**, 328-334 (2020).

65 Kallberg, M. *et al.* Template-based protein structure modeling using the RaptorX web server. *Nature Protocols* **7**, 1511-1522 (2012).

66 Holm, L. & Laakso, L. M. Dali server update. *Nucleic Acids Research* **44**, W351-W355 (2016).

Reporting summary Further information on research design is available in the Nature Reporting Summary linked to this article.

Data availability The cryo-EM density maps and the atomic model for TIM:CRY have been deposited in the EM Data Bank (EMDB: EMD-27335) and Protein Data Bank (PDB: 8DD7), respectively. The mass spectrometry proteomics data have been deposited to the ProteomeXchange Consortium via the PRIDE partner repository with the dataset identifier PXD034054. All other data is contained within the supplementary information. Reagents are available from the authors upon request.

Code availability No custom computer code was used in the study.

Acknowledgements We thank Qin Fu and Sheng Zhang of the Proteomics and Metabolomics Facility of Cornell University for providing the mass spectrometry data; Katherine Spoth and Mariena Silvestray-Ramos for help with EM instrumentation; Yitong Li for suggesting use of the ALFA Tag and experimental assistance, Greg Merz, Thuy-Tien Nguyen, and Cody Aplin for general aid; and Richard Cerione and Michael Young for helpful feedback. Figures 1A, inlet in 2B,

4D, and S1 were created with BioRender.com. This work was supported by NIH grants R35GM122535 to BRC and 1S10 OD017992-01 for the Orbitrap Fusion mass spectrometer. This work made use of the Cornell Center for Materials Research Shared Facilities which are supported through the NSF (DMR-1719875).

Author contributions All authors contributed to each aspect of the study, but primarily, C.L., and C.C.D developed the SWFTI assay, C.L. performed CRY:TIM binding assays, C.L. assisted by C.C.D. developed methods to produce the CRY:TIM complex, C.L. prepared the complex for structural analysis. S.F. prepared samples for cryo-EM, collected and processed cryo-EM data, S.F. and B.R.C. built the CRY:TIM model, C.L., S.F., and B.R.C. analyzed the structure, C.L., S.F., C.C.D, and B.R.C. wrote the manuscript, B.R.C. conceived of and oversaw the project.

Corresponding author

Correspondence to Brian R. Crane bc69@cornell.edu

Competing interests The authors declare that they have no competing interests.

714 **Figure Legends**

715

716 **Figure 1. Cryo-EM structure of the CRY:TIM complex.** (**a**) Drosophila Cryptochrome (CRY)
717 entrains the circadian clock by initiating degradation of Timeless (TIM) in light. Jetlag (JET),
718 Period (PER), Doubletime (DB), Cycle (CYC), Clock (CLK) and Importin-α1 (IMPα1) compose
719 the core circadian oscillator. (**b**) CRY:TIM docked into the electron density map. Dark-state CRY
720 shown at the bottom (grey, PDB ID: 4GU5). (**c**) Domain arrangements and key regions of CRY
721 and TIM. Features of TIM: CRY-binding domains (CRY-BD1, 1-234, CRY-BD2, 1133-1398),
722 serine/threonine-rich region (ST, 270-290) with key phosphorylation sites starred (S274, T278,
723 T282, S286 and S290), ARM1 (1-248), ARM2 (578-866), nuclear localization sequence (NLS,
724 545-578), Parp-1 binding domain (PAB, 986-1142; TIM-C, 1051-1096), 23 residue L-TIM
725 extension (L, (23aa)), disordered regions are dashed. Features of CRY: Phosphate binding loop
726 (PL, 249-263), Protrusion motif (PM, 288-306), C-terminal lid (CL, 420-446), C-terminal tail
727 (CTT, 519-542, absent in CRYΔ). (**d**) N-terminus of TIM inserts into the primary flavin binding
728 pocket. 2.4 Å resolution local electron density is shown with notable hydrogen bonds (yellow
729 dashes) and hydrophobic contacts (green circle). (**e**) Interface between CRY and TIM (blue
730 shaded area), TIM groove peptide (in navy blue) and peripheral helix (fitted with 1209-1219
731 provisionally, blue). Inset shows the interactions between TIM 1209-1219 and CRY
732 superimposed with electron density.

733

734 **Figure 2. Conformational changes of FAD to the CRY C-terminal coupled motif upon**
735 **binding TIM.** (**a**) CRY:TIM (CRY, yellow; TIM, blue) in superposition with dark-state CRY. The
736 N-terminus of TIM replaces the CRY CTT (red), as depicted in the schematic below. Structural
737 elements designated as in **Figure 1**. A CTT-like sequence on TIM (617-626) that in isolation
738 binds light-state CRY[13] locates in the ARM core remote from the interface and is thus unlikely to
739 be a binding determinant. (**b**) The phosphate binding loop (dark pink) collapses into the flavin
740 pocket and N253 and E254 hydrogen bond (yellow dashes) with the FAD diphosphate
741 conformation (red, orange) that differs substantially from that of the dark state (white bonds). (**c**)
742 R237 replaces the Mg^{2+} counter ion and H377 anchors the new position of the loop. The D410-
743 R381 salt bridge (top) appears to break in response to the new conformation of the ribose
744 backbone (bottom). Reduced side-chain density of R381 suggests increased flexibility in the
745 TIM complex.

746

747 **Figure 3. Conservation of recognition modes by CRY family members.** (**a**) The interaction
748 of CRY with TIM corresponds closely to how 6-4 photolyase recognizes the 6-4 pyrimidine
749 lesion in damaged DNA (PDB ID:3CVU). TIM Leu4 and Leu5 superimpose on the crosslinked
750 bases and the TIM ARM1- α1 polypeptide closely follows the path of 5'-to-3' strand-separated
751 DNA. (**b**) The TIM and FAD contacts of CRY mimic the interaction of apo-mCRY with the C-
752 terminus of the FBXL3 E3 ligase (PDB ID: 4I6J).
753
754 **Figure 4. A structural basis for regulation of TIM nuclear entry.** (**a**) Electron density (dark
755 blue) for an extended polypeptide resides within a groove wherein members of the β-catenin
756 and α-importin proteins bind their target sequences. (**b**) The TIM groove peptide density shown
757 with the sequence assignment S283-T303. The peptide interacts with β-catenin-conserved Asn
758 and Arg residues and buries residues important for importin-α1 binding (T90 and P92). (**c**)
759 DSSO-mediated lysine crosslinking patterns of disordered residues K313 and K238 shown on
760 the TIM structure. K313 and K328 produce a pattern of crosslinking that localizes them to a
761 position consistent with placement of the S283-T303 groove peptide. The TIM NLS lies in a
762 helix adjacent to the groove but does not occlude T90 and P92. (**d**) Schematic of proposed
763 nuclear entry mechanism of TIM. Phosphorylation of the TIM-ST region by SGG and CK2
764 releases the ST region from TIM groove to expose TIM T90 and P92. Importin-α1 binds TIM
765 adjacent to Thr90 and Pro92, while also binding the TIM NLS within a structurally analogous
766 ARM groove of its own.
767

768 **Extended Data Figure Legends**

769 **Extended Data Figure 1. CRY:TIM purification and cryo-EM workflow.** Purification of
770 CRY:TIM complexes for cryo-EM. (a) SDS-PAGE gel showing complex after elution from the
771 ALFA resin, followed by crosslinking, followed by SEC. (b) SEC trace of purified complex, peak I:
772 aggregates, peak II: CRY-TIM complex, and peak III: excessive ALFA peptide. (c) Processing
773 workflow for CRY:TIM collected on a Talos Arctica (Thermo Fischer Scientific) operated at 200
774 keV using a Gatan K3 direct electron camera. The red box indicates the final reconstruction in
775 this study. Data processing was carried out in CryoSparc and RELION. Motion Correlation was
776 performed by RELION (MotionCor2); with Contrast Transfer Function (CTF) applied in CryoSparc.
777 Topaz was used for particle classification. Overall resolution determination in CryoSparc by Gold
778 Standard Fourier Shell Correlation (GSFSC) is shown at the mid-bottom left. Corrected values
779 give 3.30 Å overall resolution. Local resolution exceeds 2.5 Å, as shown on the bottom right.

780 Particle orientational sampling is reasonably uniform as shown at the bottom left. Number of
781 particles (images) holding a given azimuthal and elevation angle are indicated in the 2-
782 dimensional histogram.

783 **Extended Data Figure 2. TIM domain construction and secondary structure assignments**.
784 Domain construction and secondary structure assignments of TIM.
785

786 **Extended Data Figure 3. CRY domain construction and secondary structure assignments.**
787 Domain construction and secondary structure assignments of CRY.
788

789 **Extended Data Figure 4. Key interactions at the CRY:TIM interface.** (a) Interactions between
790 the bottom half of TIM ARM_1-α1 with CRY. ARM1- α1 binds across CRY α14 and α17. The
791 guanidinium of CRY R446 (on α17) forms π-cation interaction with TIM Y11. TIM Y11 participates
792 in hydrophobic contacts with CRY P257, L443 and L447. On TIM α1, TIM P8 stacks against CRY
793 α12 and TIM S15 hydrogen bonds to the backbone carbonyl of CRY A442. (b) In the β-hairpin
794 connecting ARM_1- α1 to ARM_1- α2 E21 salt-bridges to R474 and C19 interacts with K445. (c)
795 Interactions of the CRY protrusion motif. TIM R109, F113, and H110 interact with the protrusion
796 motif of CRY. TIM ARM_2-α3 H110 stacks with CRY H307. Four Met residues (M179, M181 M182,
797 M185) in the ARM_3-α2-α3 loop provide side-chain interactions with the tip of the CRY protrusion
798 motif. The CRY α10 helix lengthens to residue A295 compared to the dark state and the following
799 300-306 residues interact directly with ARM_2-α3. (d) Interactions of the CRY C-terminal lid and
800 α20 helix. The restructured C-terminal lid interacts with residues on TIM ARM_1- α2. For examples,
801 L34 make a hydrophobic contact with I436 and E37 hydrogen bonds to the backbone of S434. At
802 the end of ARM_1- α2, Asn30 contacts the N-terminal end of CRY α20. A DSSO crosslink observed
803 between Lys510 on CRY a20 and Lys41 on ARM1-α3 is fully consistent with the observed
804 interface.
805

806 **Extended Data Figure 5. Changes in flavin binding pocket for CRY dark and bound states.**
807 Comparison of the flavin pocket in CRY:TIM compared to in dark-state CRY (PDB 4GU5). (a) In
808 CRY:TIM, Y250 and L251 interact with the FAD pocket and make space for the top of TIM ARM_1-
809 α3 to insert F58 behind the new conformation of the phosphate-binding loop. (b) The FAD adenine
810 ring of CRY:TIM slides 1.5 Å relative to the unbound structure. CRY F318 shifts away from its
811 original position and harbors helix α11 to compensate for the FAD adenine ring adjustment,

following the protrusion motif. (c) G311 swivels away from the inserted TIM L4. New diphosphate conformations cause rearrangement of the CRY 262-to-264 loop.

Extended Data Figure 6. Exit channel at the CRY:TIM interface and CRY secondary pocket. (a) Putative exit channel for the additional 23 N-terminal residues of L-TIM. The first residue of TIM (M1) is colored as red. A solvent accessible channel at the interface between the two proteins is marked as the green arrow. (b) Electron density for the secondary binding pocket of CRY where antenna cofactors bind in photolyases and mCRY interact with other Clock proteins (**red** box) CRY (**yellow**), TIM (**periwinkle blue**), TIM 1163-1174 (**blue**), TIM groove (**navy blue**). Although the pocket is well formed, there is no obvious density for additional moieties.

Extended Data Figure 7. TIM peripheral helix and groove peptide fitting to the electron density map and associated Q-scores. (a) Real-space electron density fitting metrics for the top scoring sequence assignments for the TIM peripheral helix. Real space density agreements were calculated in Q-scores and are shown above for sidechains and below for mainchains. One of the top scoring segments, residues 1209-1219 (top left) was also predicted by AlphaFold2.1 to interact with CRY at the position of the observed electron density, the model confidence pLDDT scores for this segment are given at the top right. (b) Real-space electron density fitting metrics for the top scoring sequence assignments for the TIM groove-binding polypeptide. Real space density agreements were calculated in Q-scores and are shown above for sidechains and below for mainchains. The TIM groove binding polypetide was tested in both directions.

Extended Data Figure 8. Relative binding affinities between fragments of TIM and CRY H377L by the SWFTI assay. (a) The CRY H377L variant acts as a constitutive light-activated state and enhances binding affinity for TIM by stabilizing the TIM-binding conformation of CRY[16]. H377L thereby increases TIM expression levels and facilitates detection of weaker binding variants. Mean ± standard error is shown for sample size = 3, from different biological replicates. One-way ANOVA with post-hoc Tukey HSD test was used to determine p values. (b) Pull down results of CRY-H377L with TIM-1133-1398. CRY-H377L interacts with the C-terminal regions of TIM. Gel lanes containing replicates or unrelated samples are not shown. (c) Quantification of the binding strength between CRY-H377L and TIM (1133-1398) compared to the negative control (CRY-H377L only with the same amount of resin). The binding strength is defined as the amount of CRY on the resin divided by the amount of CRY in the lysate sample. The negative control is normalized to 1. Mean ± standard error is shown for sample size = 3, from different biological

replicates. Two-tailed unpaired t-test was used to determine p value. Binding affinities could not be derived from this experiment owing to the challenge of producing excessive CRY relative to TIM 1133-1398.

Extended Data Figure 9. Comparisons of structural features in the CRY:TIM complex to those of CRY and TIM homologues. (a) Structural comparison of CRY:TIM with mammalian CRY bound with mammalian PER. TIM 1163-1174 (**blue**) follows the backbone trace of mPER (CRYΔ (**yellow**), TIM BD2 1163-1174 (**blue**)). 4CT0: Crystal Structure of Mouse Cryptochrome1 in Complex with Period2 (**magenta**). 4U8H: Crystal Structure of Mammalian Period-Cryptochrome Complex (**green**). 6OF7: Crystal structure of the CRY1-PER2 complex (**orange red**). (b) Structural comparison of CRY:TIM (CRY (**yellow**), TIM (**periwinkle blue**), TIM 1163-1174 (**blue**), TIM groove peptide (**navy blue**)) with the crystal structure of the N-terminal domain of human Timeless (PDB ID: 5MQI, **salmon**). Note that mammalian TIM does not contain the N-terminal residues that bind into the CRY flavin pocket. (c) Structural superposition of TIM PAB (PARP-1 binding) domain and PARP-1 model with the structure of human TIM PAB bound to the PARP-1 catalytic domain (4XHU). Red box highlights the additional TIM α-helix (PAB-C-α4) that is incompatible with the interface formed by human PARP-1 and TIM PARP-1 binding. The TIM C region conserved across TIM proteins (residue 1051-1096) is also shown. TIM (this study, **periwinkle blue**), *Drosophila* PARP-1 (AlphaFold2.1 model: **dark red**) 4XHU (PAB:**green**, PARP-1:**orange**). (d) Superposition of TIM and Tof1 within the replisome.

Extended Data Figure 10. Interactions between TIM and its homologs with extended polypeptides in their respective ARM grooves in relation to crosslinking map of CRY:TIM. (a) Sequence alignment of top TIM structural homologs. Boxes outline the conserved R-XXX-N and RN residues within the ARM motifs that interact with the extended polypeptide chains of binding partners. Protein Data Bank (PDB) codes are shown on the left. (b) The extended peptide bound in the TIM groove resembles interactions found in other ARM-repeat proteins such as Importin-α1, β-catenin, and yeast TIM proteins. ARM-repeat proteins were structurally superimposed by their ARM-repeat cores to show the alignment of the extended peptides that bind in the crescent groove common to the family. For clarity only the groove peptides are displaced. Extended polypeptides found in yeast TOF1 (6SKL) and β-catenin (3IFQ) and TIM travel on the same lateral axis anti-parallel to the other importin- α, β-catenin, and TIM protein homologues. The PDB labels indicate the N-terminus of the loop. 6SKL: Cryo-EM structure of the CMG Fork Protection Complex at a replication fork - Conformation 1 (lavender), 3IFQ: Interaction

880 of plakoglobin and β-catenin with desmosomal cadherins (**gold**), 1JDH: Crystal structure of β-
881 catenin and htcf-4 (**purple**), 3L3Q: Mouse importin $\boldsymbol{\alpha}$-pepTM NLS peptide complex (gray), 3KND:
882 TPX2:importin-αlpha complex (**magenta**), 1IQ1: Crystal structure of the importin-$\boldsymbol{\alpha}$(44-54)-
883 importin-$\boldsymbol{\alpha}$(70-529) complex (**salmon**), 3UKX: Mouse importin-$\boldsymbol{\alpha}$:Bimax2 peptide complex (**sky**
884 **blue**). (c) Map of DSSO lysine residue crosslinking defined by mass spectroscopy for the
885 CRY:TIM complex. For the LysC+trypsin digested sample, although +2-charged peptides were
886 excluded in the analysis, 59.79% sequence coverage for CRY and 49.81% for TIM were obtained.
887 For the LysC+trypsin+GluC digested sample, 25.07% sequence coverage was obtained for CRY
888 and 25.53% sequence coverage was obtained for TIM. Summary of the cross-links are given in
889 the attached excel files and the raw data has been submitted to the PRIDE database.

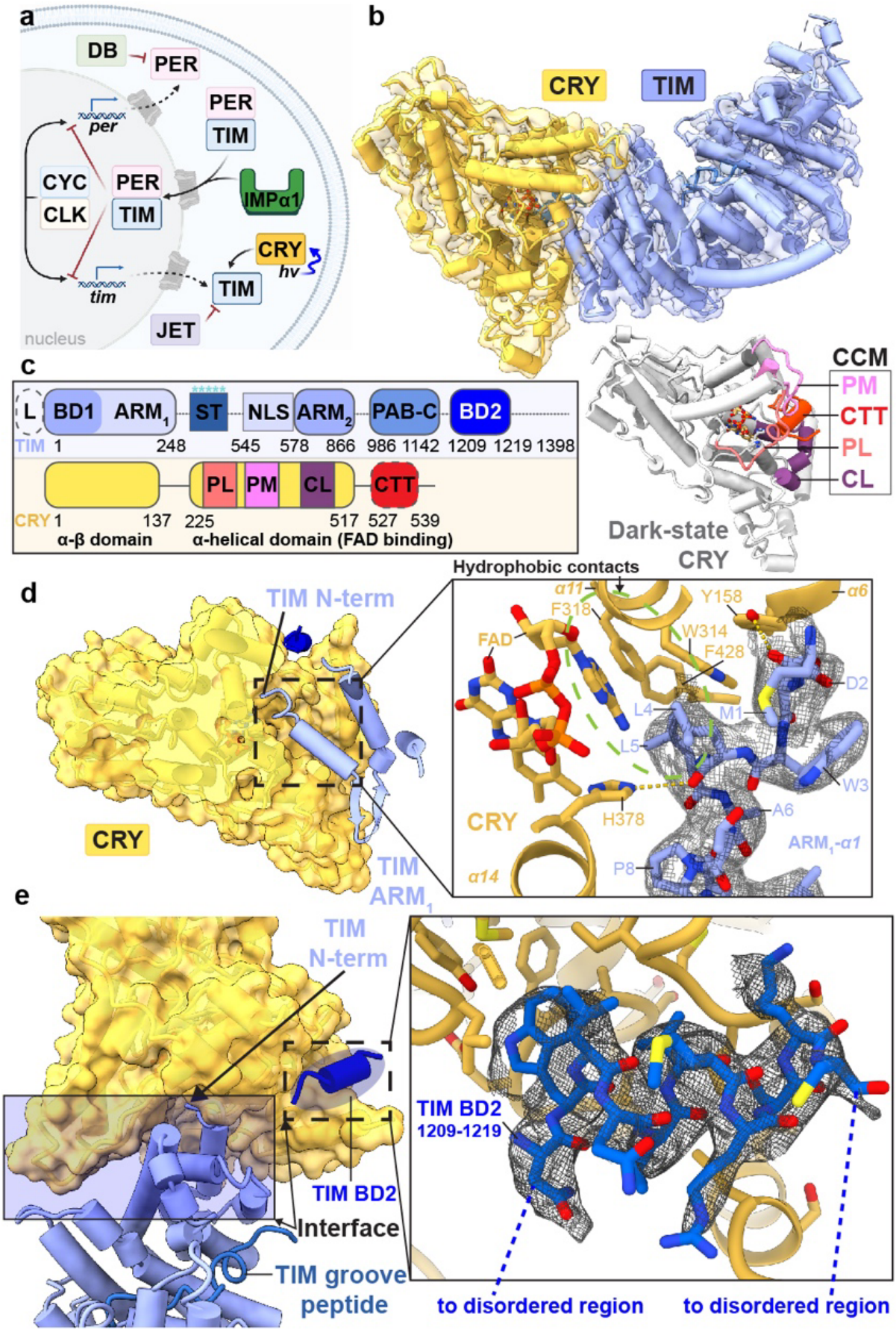
a
DB
PER
PER
TIM
per
CYC
CLK
PER
TIM
IMPα1
CRY
hv
TIM
tim
JET
nucleus
b
CRY
TIM
c
L
BD1
ARM1
ST
NLS
ARM2
PAB-C
BD2
TIM 1 248 545 578 866 986 1142 1209 1219 1398
PL
PM
CL
CTT
CRY 1 137 225 517 527 539
α-β domain
α-helical domain (FAD binding)
CCM
PM
CTT
PL
CL
Dark-state CRY
d
TIM N-term
CRY
TIM ARM1
Hydrophobic contacts
α11
F318
FAD
Y158
α6
W314
F428
D2
L4
M1
L5
W3
CRY
H378
A6
ARM1-α1
α14
P8
e
TIM N-term
TIM BD2
Interface
TIM groove peptide
TIM BD2
1209-1219
to disordered region
to disordered region

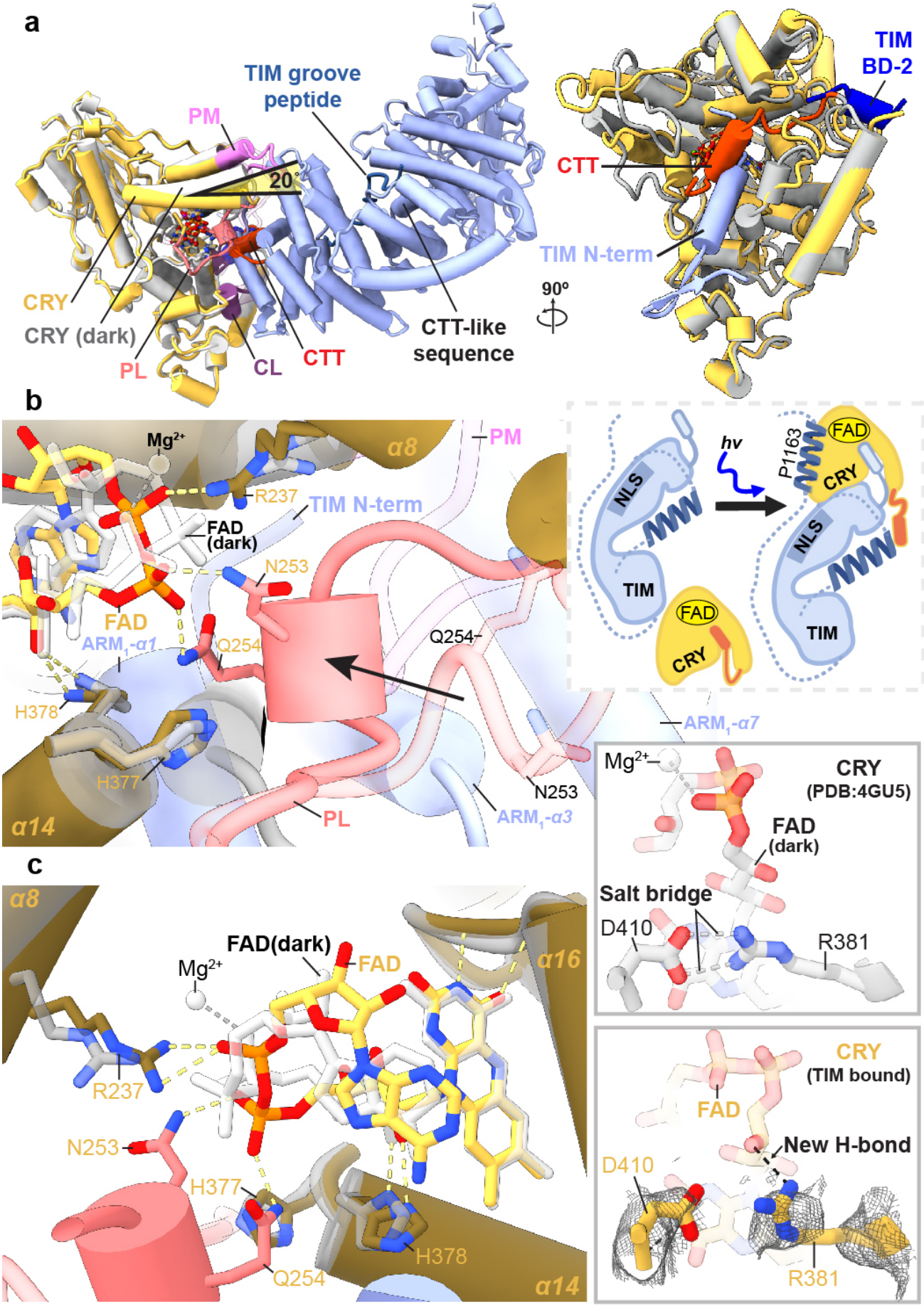
a
TIM groove peptide
PM
20°
CRY
CRY (dark)
PL
CL
CTT
CTT-like sequence
TIM BD-2
CTT
TIM N-term
90°
b
Mg2+
α8
PM
R237
TIM N-term
FAD (dark)
N253
FAD
ARM1-α1
Q254
Q254
H378
H377
α14
PL
ARM1-α3
N253
ARM1-α7
hv
P1163
FAD
CRY
NLS
TIM
FAD
CRY
NLS
TIM
Mg2+
CRY (PDB:4GU5)
FAD (dark)
Salt bridge
D410
R381
c
α8
FAD(dark)
Mg2+
FAD
α16
R237
N253
H377
H378
Q254
α14
CRY (TIM bound)
FAD
New H-bond
D410
R381

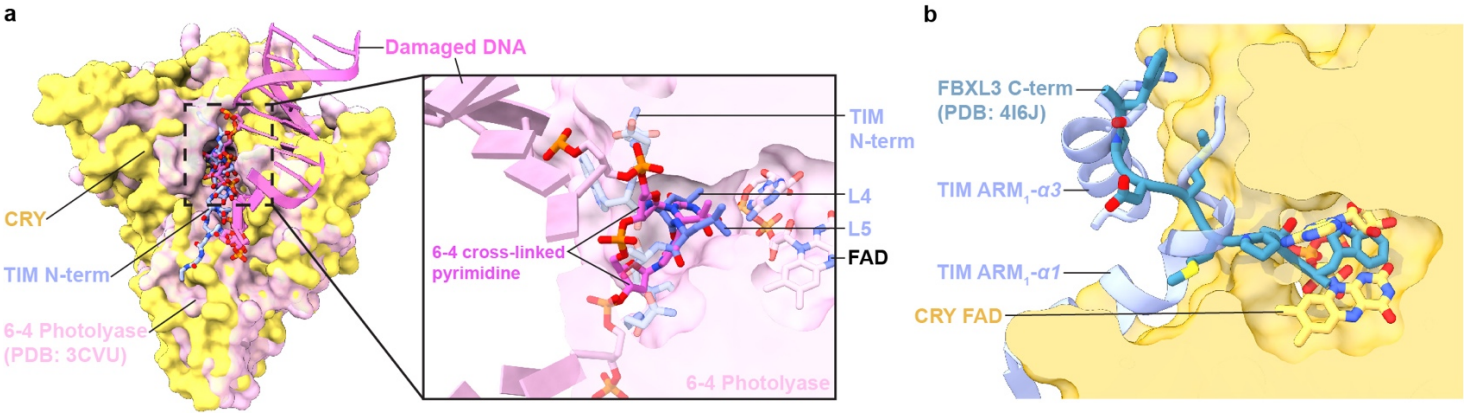
a
Damaged DNA
CRY
TIM N-term
6-4 Photolyase
(PDB: 3CVU)
TIM
N-term
L4
L5
FAD
6-4 cross-linked
pyrimidine
6-4 Photolyase
b
FBXL3 C-term
(PDB: 4I6J)
TIM ARM1-α3
TIM ARM1-α1
CRY FAD

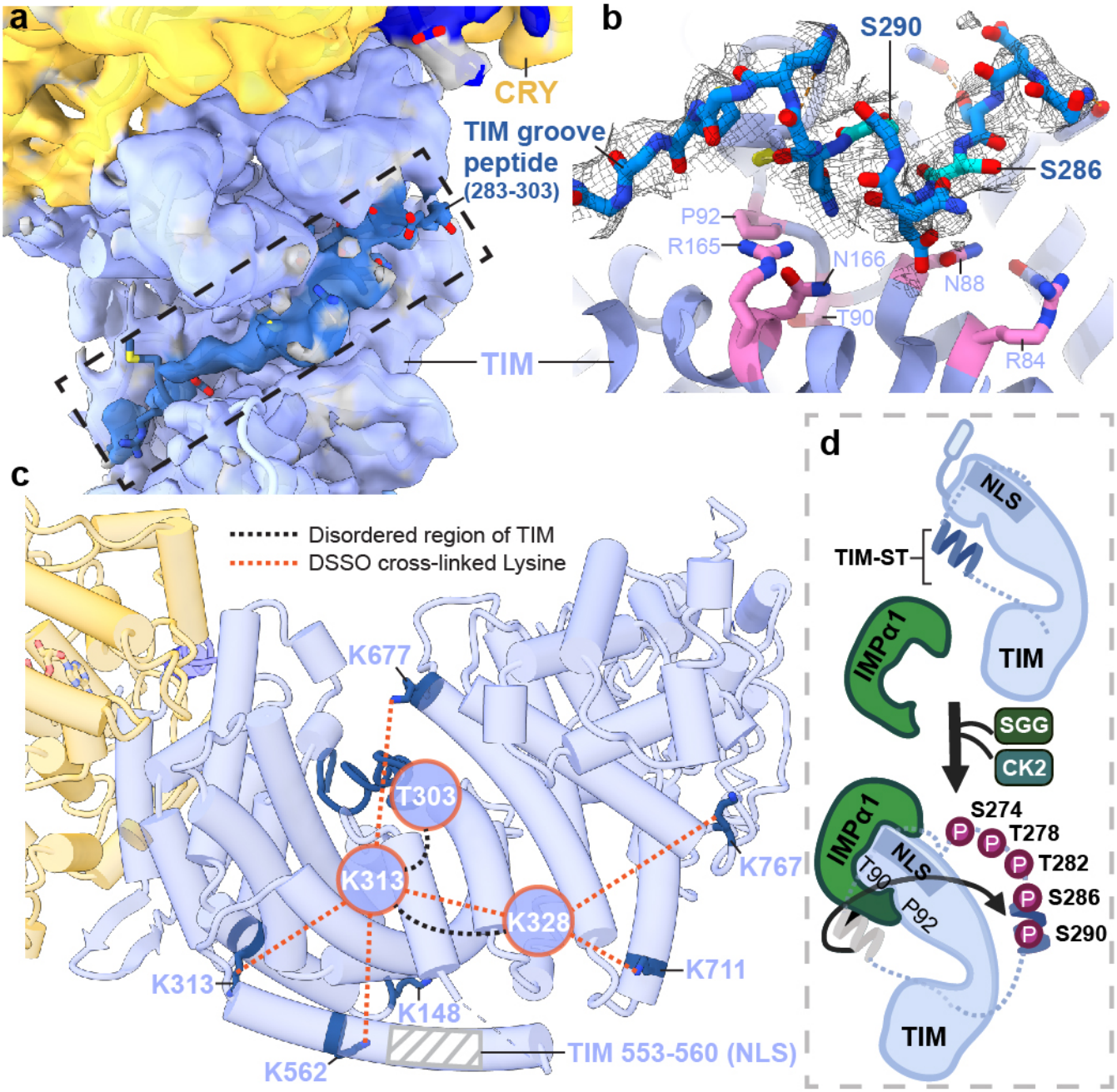
a
CRY
TIM groove
peptide
(283-303)
TIM
b
S290
S286
P92
R165
N166
N88
T90
R84
c
Disordered region of TIM
DSSO cross-linked Lysine
K677
T303
K313
K328
K767
K711
K313
K148
K562
TIM 553-560 (NLS)
d
NLS
TIM-ST
IMPα1
TIM
SGG
CK2
IMPα1
NLS
T90
P92
S274
T278
T282
S286
S290
TIM

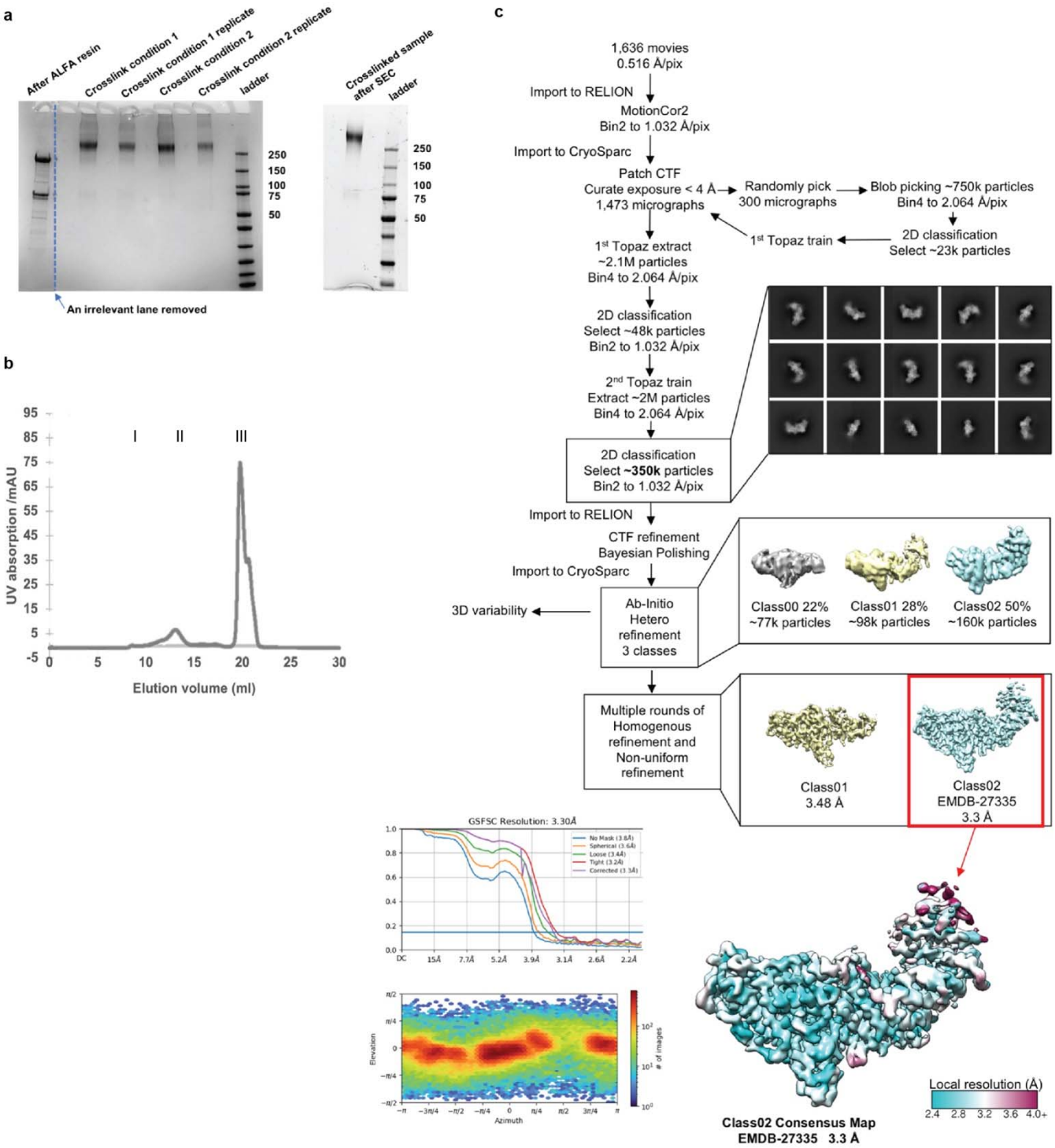

Extended Data Fig. 1

Extended Data Figure 1. CRY:TIM purification and cryo-EM workflow. Purification of CRY:TIM complexes for cryo-EM. (a) SDS-PAGE gel showing complex after elution from the ALFA resin, followed by crosslinking, followed by SEC. (b) SEC trace of purified complex, peak I: aggregates, peak II: CRY-TIM complex, and peak III: excessive ALFA peptide. (c) Processing workflow for CRY:TIM collected on a Talos Arctica (Thermo Fischer Scientific) operated at 200 keV using a Gatan K3 direct electron camera. The red box indicates the final reconstruction in this study. Data processing was carried out in CryoSparc and RELION. Motion Correlation was performed by RELION (MotionCor2); with Contrast Transfer Function (CTF) applied in CryoSparc. Topaz was used for particle classification. Overall resolution determination in CryoSparc by Gold Standard Fourier Shell Correlation (GSFSC) is shown at the mid-bottom left. Corrected values give 3.30 Å overall resolution. Local resolution exceeds 2.5 Å, as shown on the bottom right. Particle orientational sampling is reasonably uniform as shown at the bottom left. Number of particles (images) holding a given azimuthal and elevation angle are indicated in the 2-dimensional histogram.

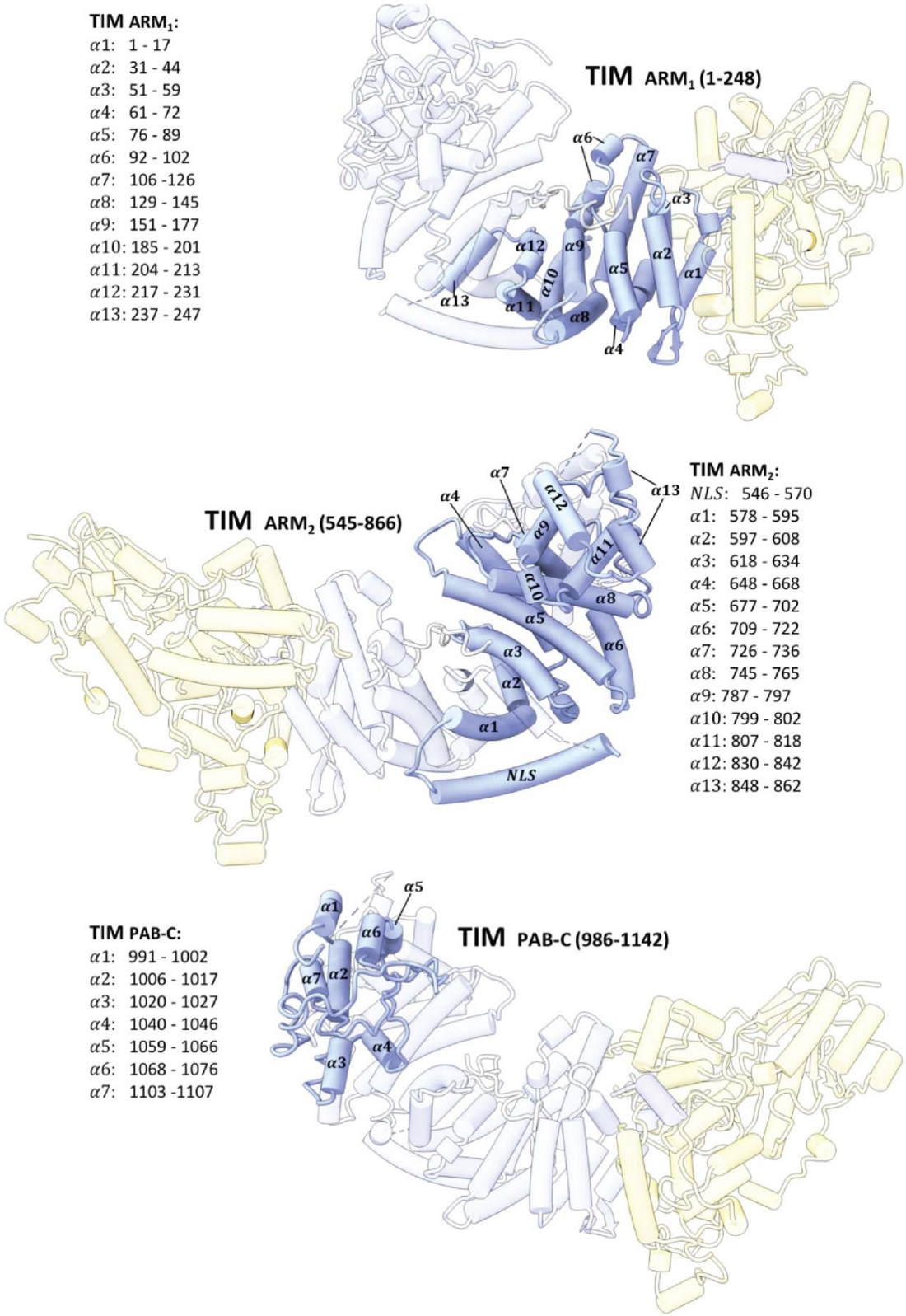

Extended Data Fig. 2

Extended Data Figure 2. TIM domain construction and secondary structure assignments. Domain construction and secondary structure assignment of TIM.

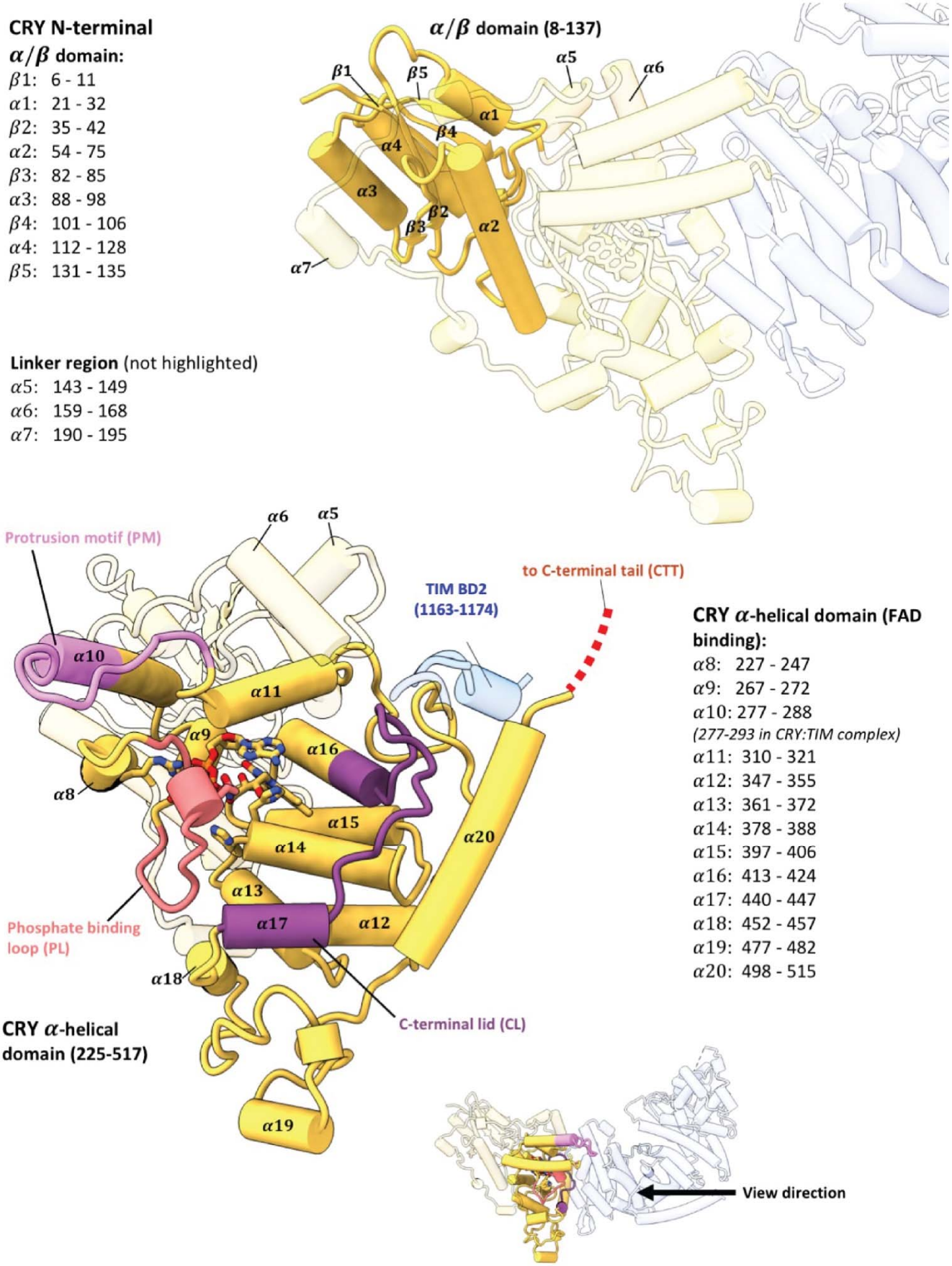

Extended Data Fig. 3

Extended Data Figure 3. CRY domain construction and secondary structure assignments. Domain construction and secondary structure assignment of CRY.

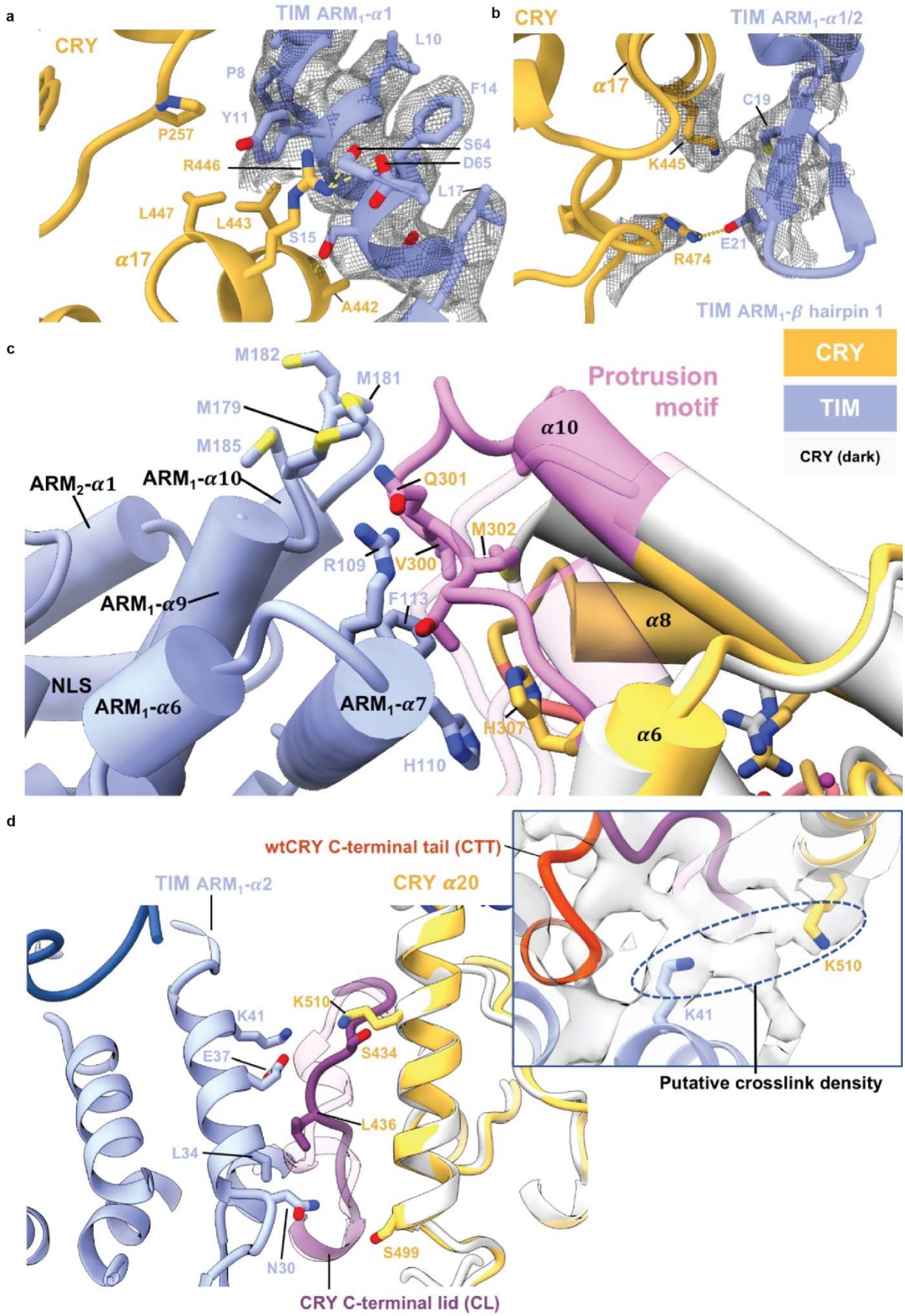

Extended Data Fig. 4

Extended Data Figure 4. Key interactions at the CRY:TIM interface. (a) Interactions between the bottom half of TIM ARM_1-α1 with CRY. ARM1- α1 binds across CRY α14 and α17. The guanidinium of CRY R446 (on α17) forms π-cation interaction with TIM Y11. TIM Y11 participates in hydrophobic contacts with CRY P257, L443 and L447. On TIM α1, TIM P8 stacks against CRY α12 and TIM S15 hydrogen bonds to the backbone carbonyl of CRY A442. (b) In the β-hairpin connecting ARM_1- α1 to ARM_1- α2 E21 salt-bridges to R474 and C19 interacts with K445. (c) Interactions of the CRY protrusion motif. TIM R109, F113, and H110 interact with the protrusion motif of CRY. TIM ARM_2-α3 H110 stacks with CRY H307. Four Met residues (M179, M181 M182, M185) in the ARM_3-α2-α3 loop provide side-chain interactions with the tip of the CRY protrusion motif. The CRY α10 helix lengthens to residue A295 compared to the dark state and the following 300-306 residues interact directly with ARM_2-α3. (d) Interactions of the CRY C-terminal lid and α20 helix. The restructured C-terminal lid interacts with residues on TIM ARM_1- α2. For examples, L34 make a hydrophobic contact with I436 and E37 hydrogen bonds to the backbone of S434. At the end of ARM_1- α2, Asn30 contacts the N-terminal end of CRY α20. A DSSO crosslink observed between Lys510 on CRY a20 and Lys41 on ARM1-α3 is fully consistent with the observed interface.

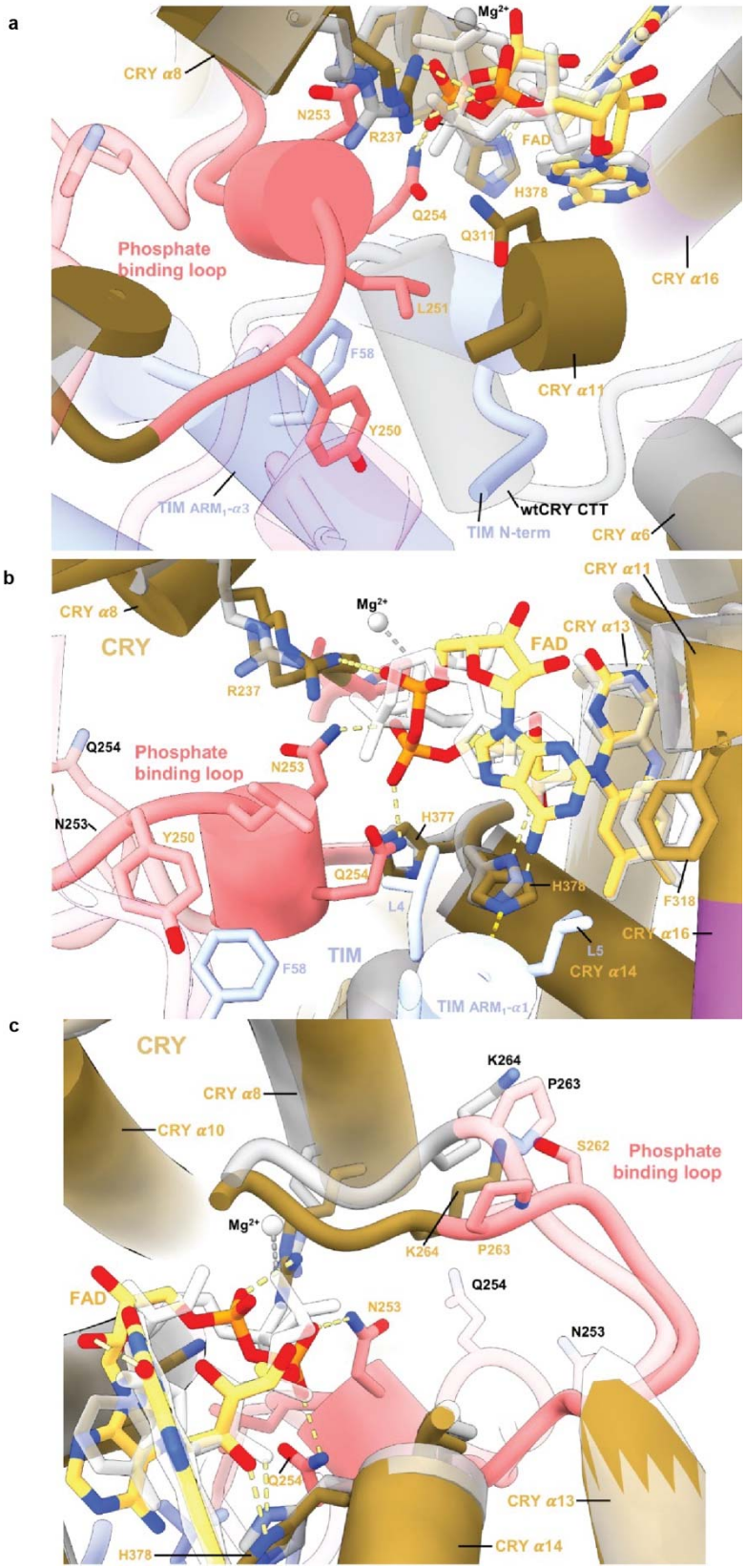

Extended Data Fig. 5

Extended Data Figure 5. Changes in flavin binding pocket for CRY dark and bound states. Comparison of the flavin pocket in CRY:TIM compared to in dark-state CRY (PDB 4GU5). (a) In CRY:TIM, Y250 and L251 interact with the FAD pocket and make space for the top of TIM ARM_1-α3 to insert F58 behind the new conformation of the phosphate-binding loop. (b) The FAD adenine ring of CRY:TIM slides 1.5 Å relative to the unbound structure. CRY F318 shifts away from its original position and harbors helix α11 to compensate for the FAD adenine ring adjustment, following the protrusion motif. (c) G311 swivels away from the inserted TIM L4. New diphosphate conformations cause rearrangement of the CRY 262-to-264 loop.

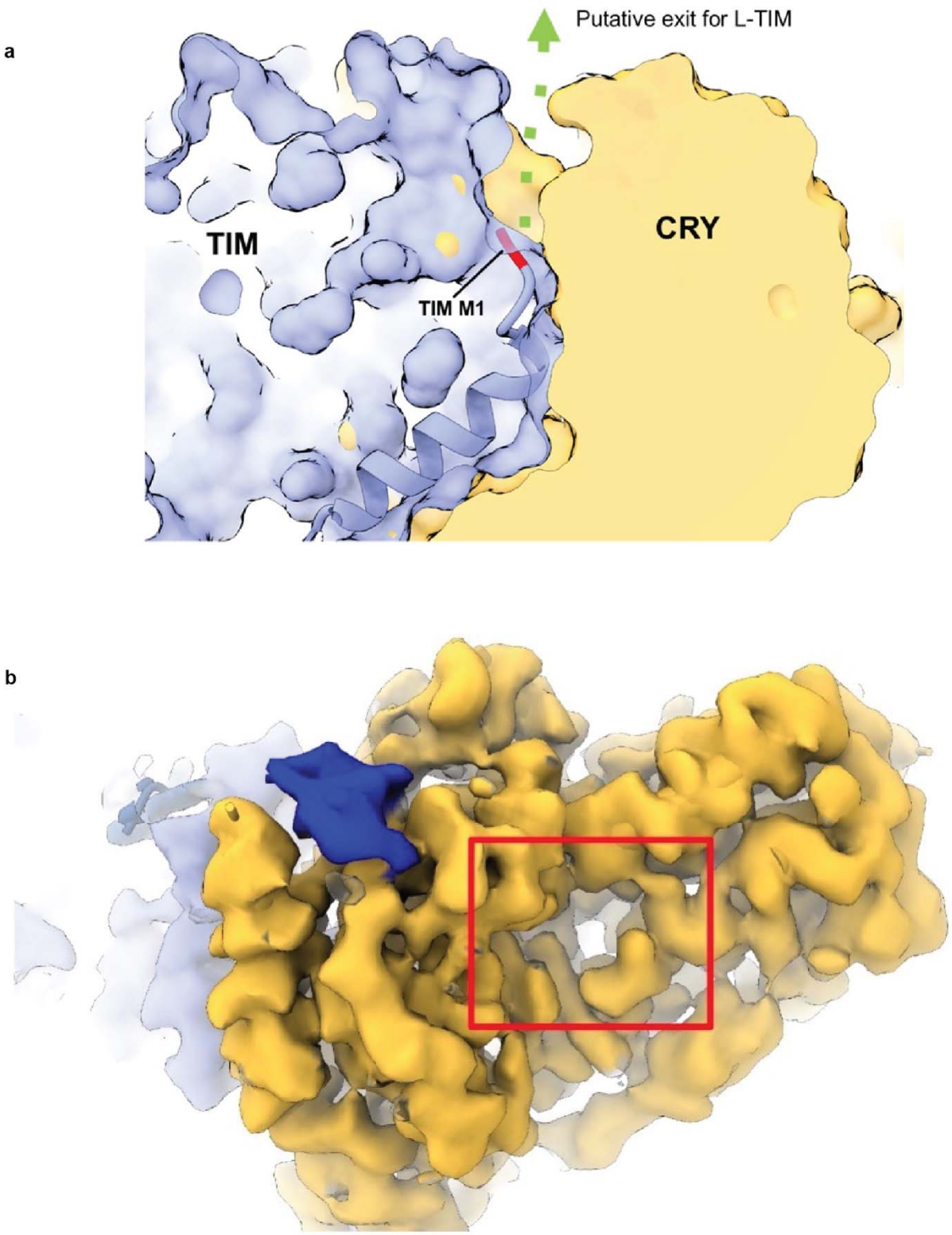

Extended Data Fig. 6

Extended Data Figure 6. Exit channel at the CRY:TIM interface and CRY secondary pocket. (a) Putative exit channel for the additional 23 N-terminal residues of L-TIM. The first residue of TIM (M1) is colored as red. A solvent accessible channel at the interface between the two proteins is marked as the green arrow. (b) Electron density for the secondary binding pocket of CRY where antenna cofactors bind in photolyases and mCRY interact with other Clock proteins (**red** box) CRY (**yellow**), TIM (**periwinkle blue**), TIM 1163-1174 (**blue**), TIM groove (**navy blue**). Although the pocket is well formed, there is no obvious density for additional moieties.

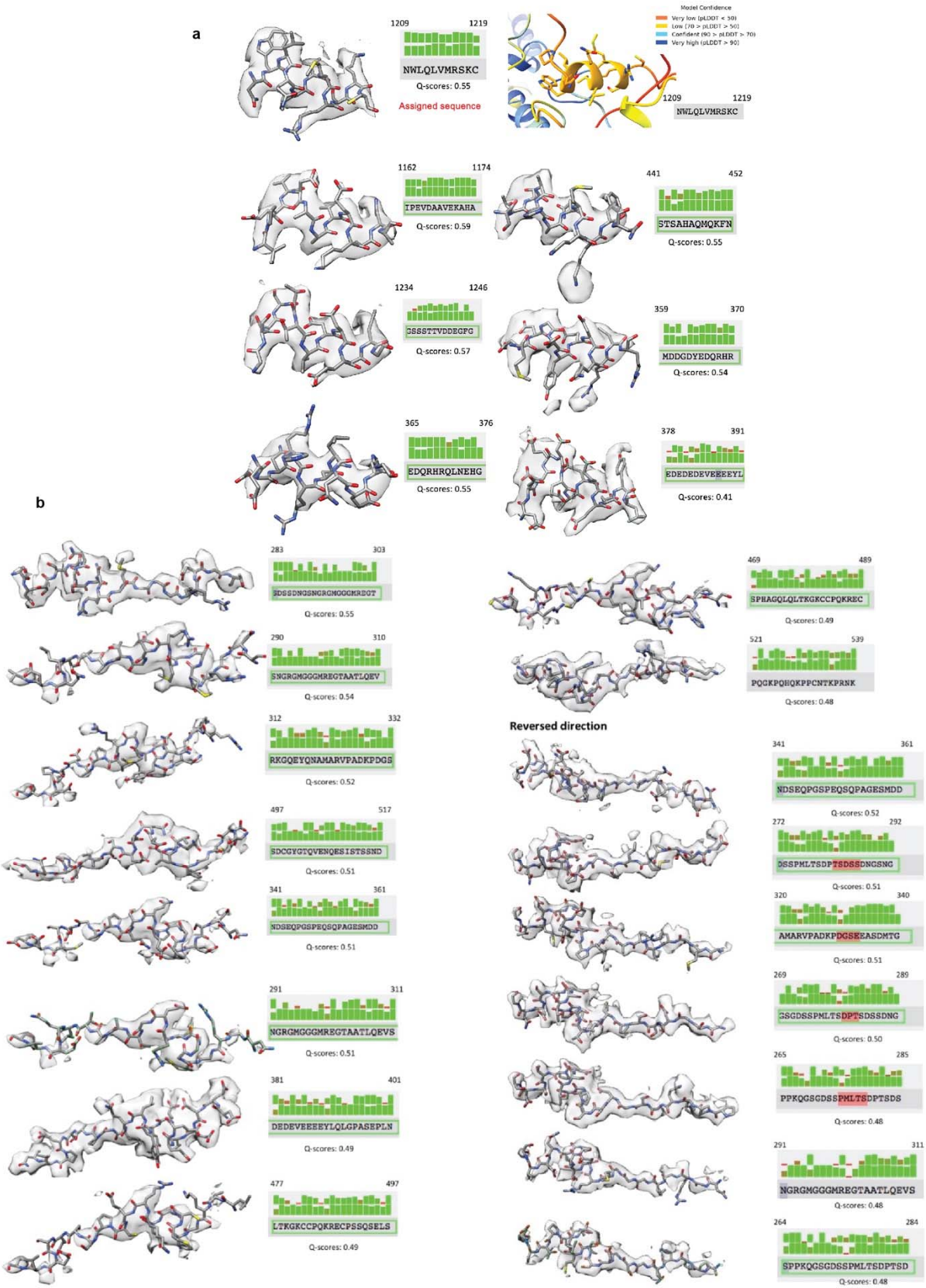

Extended Data Fig. 7

Extended Data Figure 7. TIM peripheral helix and groove peptide fitting to the electron density map and associated Q-scores. (a) Real-space electron density fitting metrics for the top scoring sequence assignments for the TIM peripheral helix. Real space density agreements were calculated in Q-scores and are shown above for sidechains and below for mainchains. One of the top scoring segments, residues 1209-1219 (top left) was also predicted by AlphaFold2.1 to interact with CRY at the position of the observed electron density, the model confidence pLDDT scores for this segment are given at the top right. (b) Real-space electron density fitting metrics for the top scoring sequence assignments for the TIM groove-binding polypeptide. Real space density agreements were calculated in Q-scores and are shown above for sidechains and below for mainchains. The TIM groove binding polypetide was tested in both directions.

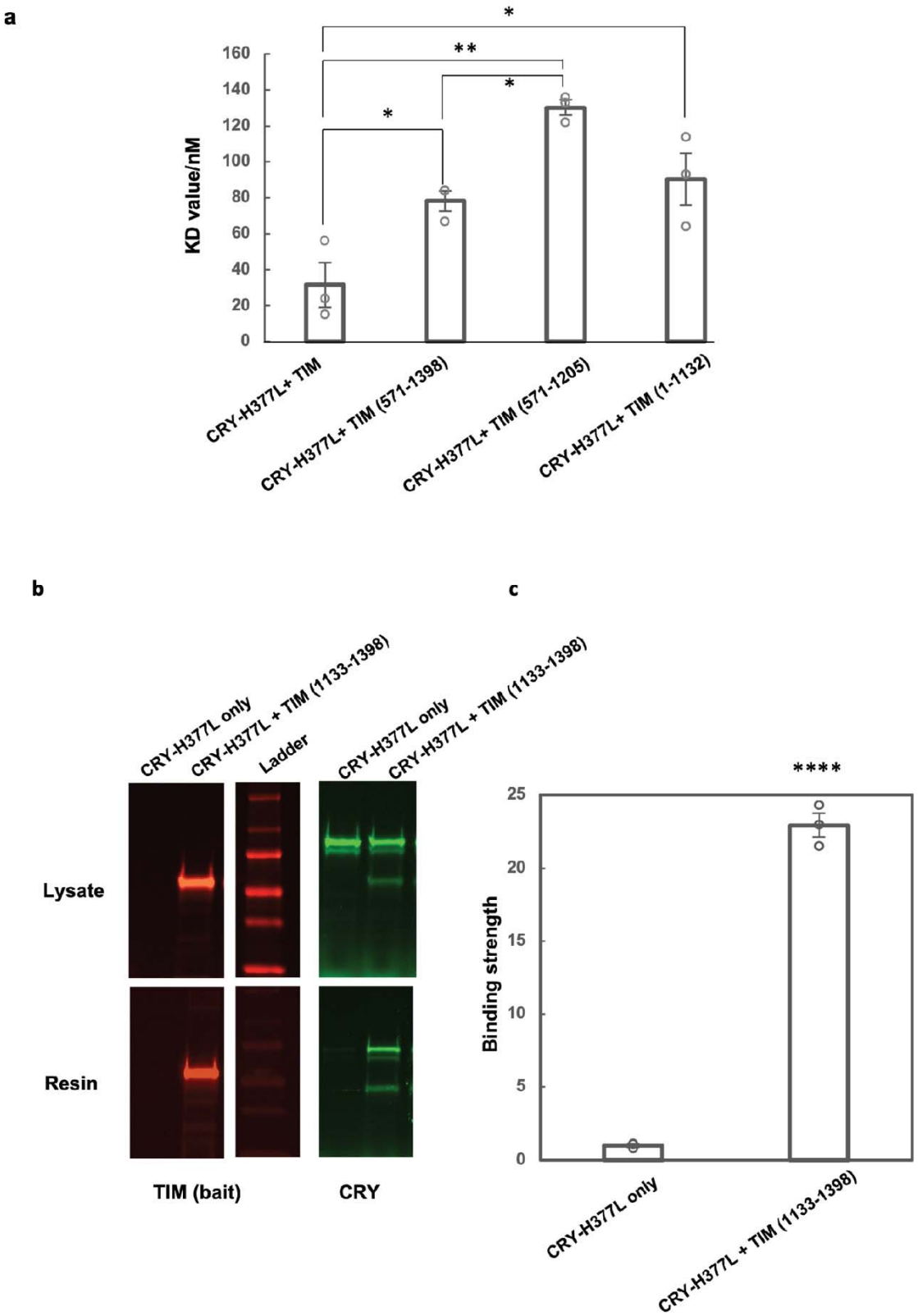

Extended Data Fig. 8

Extended Data Figure 8. Relative binding affinities between fragments of TIM and CRY H377L by the SWFTI assay. (a) The CRY H377L variant acts as a constitutive light-activated state and enhances binding affinity for TIM by stabilizing the TIM-binding conformation of CRY[13]. H377L thereby increases TIM expression levels and facilitates detection of weaker binding variants. Mean ± standard error is shown for sample size = 3, from different biological replicates. One-way ANOVA was used to analyze p value with a Tukey HSD post-hoc test for significance. * represents $p < 0.05$, ** $p < 0.01$ (b) Pull down results of CRY-H377L with TIM-1133-1398. CRY-H377L interacts with the C-terminal regions of TIM. Gel lanes containing replicates or unrelated samples are not shown. (c) Quantification of the binding strength between CRY-H377L and TIM (1133-1398) compared to the negative control (CRY-H377L only with the same amount of resin). The binding strength is defined as the amount of CRY on the resin divided by the amount of CRY in the lysate sample. The negative control is normalized to 1. Mean ± standard error is shown for sample size = 3, from different biological replicates. Two-tailed t-test yields a p value < 0.0001 (****). Binding affinities could not be derived from this experiment owing to the challenge of producing excessive CRY relative to TIM 1133-1398.

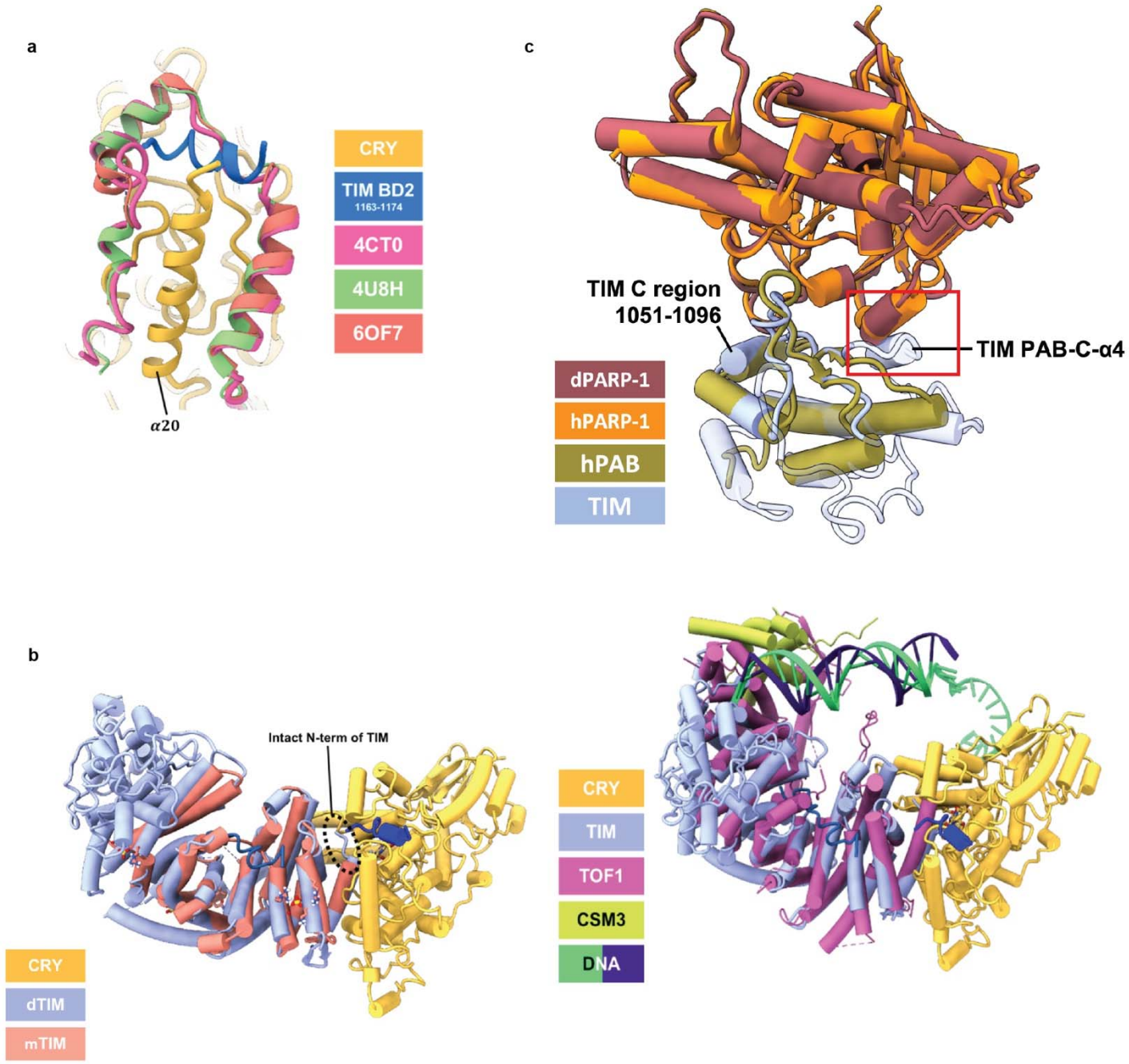

Extended Data Fig. 9

Extended Data Figure 9. Comparisons of structural features in the CRY:TIM complex to those of CRY and TIM homologues. (a) Structural comparison of CRY:TIM with mammalian CRY bound with mammalian PER. TIM 1163-1174 (**blue**) follows the backbone trace of mPER (CRYΔ (**yellow**), TIM BD2 1163-1174 (**blue**)). 4CT0: Crystal Structure of Mouse Cryptochrome1 in Complex with Period2 (**magenta**). 4U8H: Crystal Structure of Mammalian Period-Cryptochrome Complex (**green**). 6OF7: Crystal structure of the CRY1-PER2 complex (**orange red**). (b) Structural comparison of CRY:TIM (CRY (**yellow**), TIM (**periwinkle blue**), TIM 1163-1174 (**blue**), TIM groove peptide (**navy blue**)) with the crystal structure of the N-terminal domain of human Timeless (PDB ID: 5MQI, **salmon**). Note that mammalian TIM does not contain the N-terminal residues that bind into the CRY flavin pocket. (c) Structural superposition of TIM PAB (PARP-1 binding) domain and PARP-1 model with the structure of human TIM PAB bound to the PARP-1 catalytic domain (4XHU). Red box highlights the additional TIM α-helix (PAB-C-α4) that is incompatible with the interface formed by human PARP-1 and TIM PARP-1 binding. The TIM C region conserved across TIM proteins (residue 1051-1096) is also shown. TIM (this study, **periwinkle blue**), *Drosophila* PARP-1 (AlphaFold2.1 model: **dark red**) 4XHU (PAB:**green**, PARP-1:**orange**). (d) Superposition of TIM and Tof1 within the replisome.

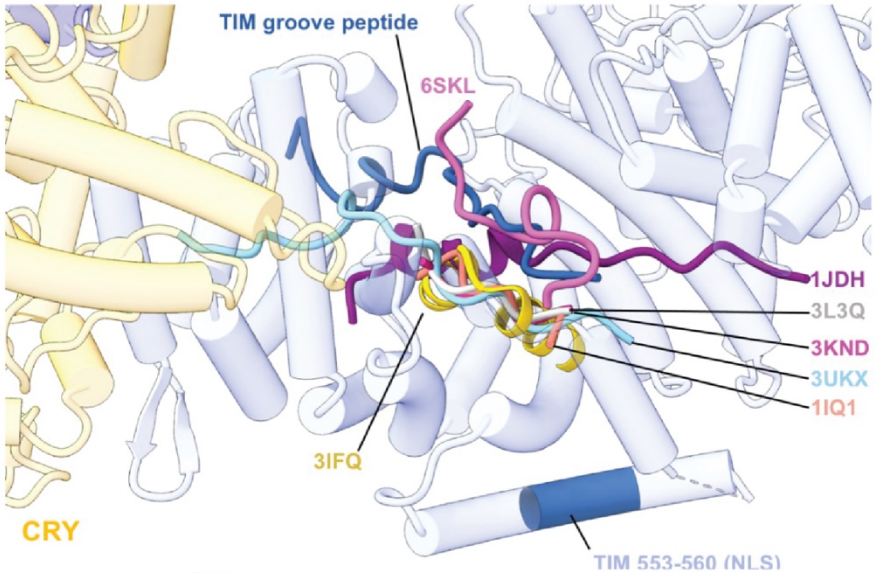

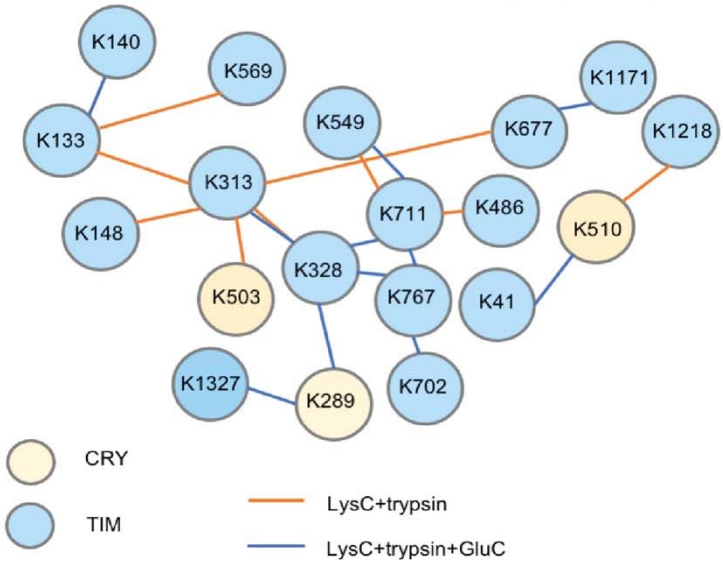

Extended Data Fig. 10

Extended Data Figure 10. Interactions between TIM and its homologs with extended polypeptides in their respective ARM grooves in relation to crosslinking map of CRY:TIM. (a) Sequence alignment of top TIM structural homologs as calculated by the DALI server[64]. Boxes outline the conserved R-XXX-N and RN residues within the ARM motifs that interact with the extended polypeptide chains of binding partners. Protein Data Bank (PDB) codes are shown on the left. (b) The extended peptide bound in the TIM groove resembles interactions found in other ARM-repeat proteins such as Importin-α1, β-catenin, and yeast TIM proteins. ARM-repeat proteins were structurally superimposed by their ARM-repeat cores to show the alignment of the extended peptides that bind in the crescent groove common to the family. For clarity only the groove peptides are displaced. Extended polypeptides found in yeast TOF1 (6SKL) and β-catenin (3IFQ) and TIM travel on the same lateral axis anti-parallel to the other importin- α, β-catenin, and TIM protein homologues. The PDB labels indicate the N-terminus of the loop. 6SKL: Cryo-EM structure of the CMG Fork Protection Complex at a replication fork - Conformation 1 (lavender), 3IFQ: Interaction of plakoglobin and β-catenin with desmosomal cadherins (**gold**), 1JDH: Crystal structure of β-catenin and htcf-4 (**purple**), 3L3Q: Mouse importin α-pepTM NLS peptide complex (gray), 3KND: TPX2:importin-αlpha complex (**magenta**), 1IQ1: Crystal structure of the importin-α(44-54)-importin-α(70-529) complex (**salmon**), 3UKX: Mouse importin-α:Bimax2 peptide complex (**sky blue**). (c) Map of DSSO lysine residue crosslinking defined by mass spectroscopy for the CRY:TIM complex. For the LysC+trypsin digested sample, although +2-charged peptides were excluded in the analysis, 59.79% sequence coverage for CRY and 49.81% for TIM were obtained. For the LysC+trypsin+GluC digested sample, 25.07% sequence coverage was obtained for CRY and 25.53% sequence coverage was obtained for TIM. Summary of the cross-links are given in the attached excel files and the raw data has been submitted to the PRIDE database.

Supplementary Information

Cryptochrome-Timeless structure reveals circadian clock timing mechanisms

Changfan Lin[†], Shi Feng[†], Cristina C. DeOliveira and Brian R. Crane
[†]Equal Contribution

Department of Chemistry and Chemical Biology, Cornell University, Ithaca, NY, 14853

Index for Supplemental Information

Table of Contents

Supplementary Methods: 3
DNA constructs: 3
Proteins Sequences: 9
Supplementary Table 1 11

Supplementary Methods:

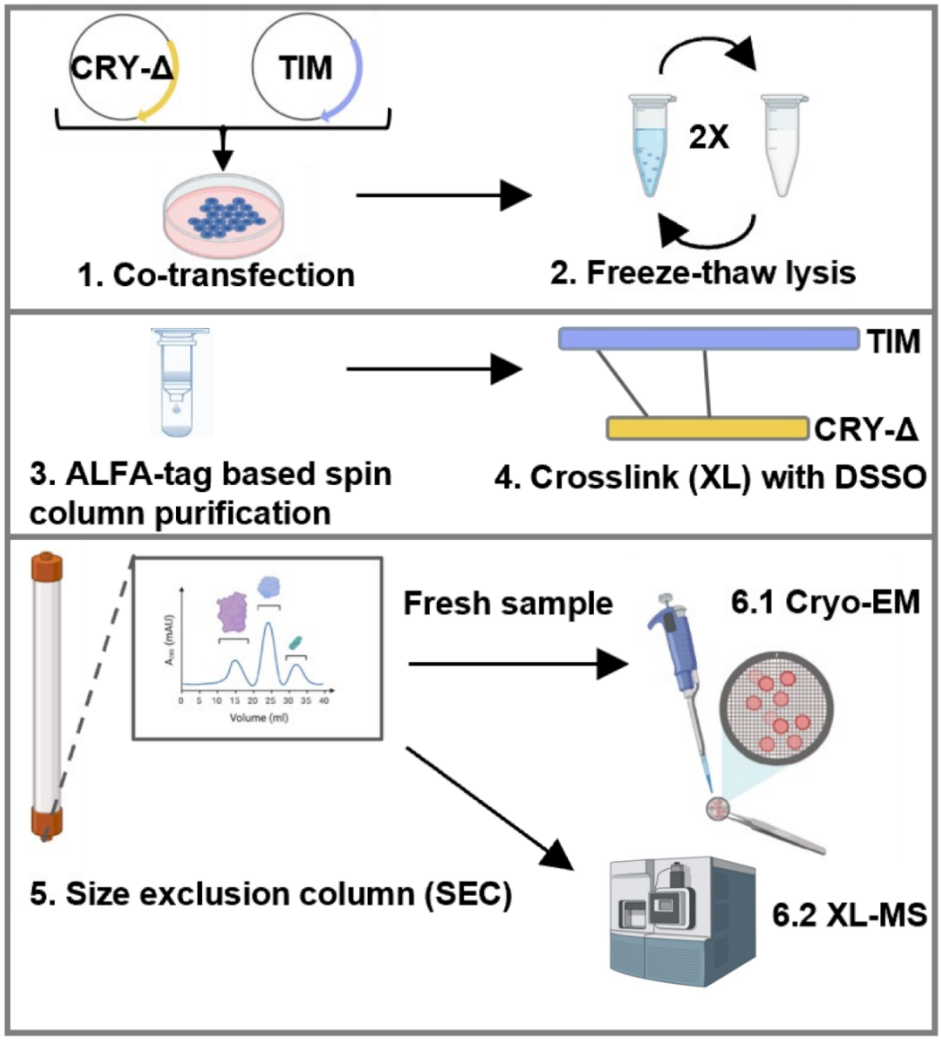

Methods Overview

Created with BioRender.com

DNA constructs:

TIM-SNAP-HA in pAC5.1 vector backbone (with unintentional minor differences from standard pAC5.1)

Key features:
Ampicillin Resistance: 171-1136
Actin 5C promoter: 1286-3794
Drosophila Kozak sequence: 3805-3812
TIM: 3809-8002
SNAP-tag: 8021-8566
HA-tag: 8576-8602

ALFA-tag: 8624-8662
Replication origin: 9471-10059

GAAGATCCTTTGATCTTTTCTACGGGGTCTGACGCTCAGTGGAACGAAAACTCACGTTAAGGGATTTTGG
TCATGAGATTATCAAAAAGGATCTTCACCTAGATCCTTTTAAATTAAAAATGAAGTTTTAAATCAATCTA
AAGTATATATGAGTAAACTTGGTCTGACAGTTACCAATGCTTAATCAGTGAGGCACCTATCTCGGCGATC
TGTCTATTTCGTTCATCCATAGTTGCCTGACTCCCCGTCGTGTAGATAACTACGATACGGGAGGGCTTAC
CATCTGGCCCCAGTGCTGCAATGATACCGCGAGACCCACGCTCACCGGCTCCAGATTTATCAGCAATAAA
CCAGCCAGCCGGAAGGGCCGAGCGCAGAAGTGGTCCTGCAACTTTATCCGCCTCCATCCAGTCTATTAAT
TGTTGCCGGGAAGCTAGAGTAAGTAGTTCGCCAGTTAATAGTTTGCGCAACGTTGTTGCCATTGCTGCAG
GCATCGTGGTGTCACGCTCGTCGTTTGGTATGGCTTCATTCAGCTCCGGTTCCCAACGATCAAGGCGAGT
TACATGATCCCCCATGTTGTGCAAAAAAGCGGTTAGCTCCTTCGGTCCTCCGATCGTTGTCAGAAGTAAG
TTGGCCGCAGTGTTATCACTCATGGTTATGGCAGCACTGCATAATTCTCTTACTGTCATGCCATCCGTAA
GATGCTTTTCTGTGACTGGTGAGTACTCAACCAAGTCATTCTGAGAATAGTGTATGCGGCGACCGAGTTG
CTCTTGCCCGGCGTCAACACGGGATAATACCGCGCCACATAGCAGAACTTTAAAAGTGCTCATCATTGGA
AAACGTTCTTCGGGGCGAAAACTCTCAAGGATCTTACCGCTGTTGAGATCCAGTTCGATGTAACCCACTC
GTGCACCCAACTGATCTTCAGCATCTTTTACTTTCACCAGCGTTTCTGGGTGAGCAAAAACAGGAAGGCA
AAATGCCGCAAAAAAGGGAATAAGGGCGACACGGAAATGTTGAATACTCATACTCTTCCTTTTTCAATAT
TATTGAAGCATTTATCAGGGTTATTGTCTCATGAGCGGATACATATTTGAATGTATTTAGAAAAATAAAC
AAATAGGGGTTCCGCGCACATTTCCCCGAAAAGTGCCACCTGACGTCTAAGAAACCATTATTATCATGAC
ATTAACCTATAAAAATAGGCGTATCACGAGGCCCTTTCGTCTTCAAGAATTAATTCTATATTCTAAAAAC
ACAAATGATACTTCTAAAAAAAAATCATGAATGGCATCAACTCTGAATCAAATCTTTGCAGATGCACCTA
CTTCTCATTTCCACTGTCACATCATTTTTCCAGATCTCGCTGCCTGTTATGTGGCCCACAAACCAAGACA
CGTTTTATGGCCATTAAAGCTGGCTGATCGTCGCCAAACACCAAATACATAATGAATATGTACACATTCG
AGAAAGAAGCGATCAAAGAAGCGTCTTCGGGCGGAGTAGGAGAATGCGGAGGAGAAGGAGAACGAGCTGA
TCTAGTATCTCTCCACAATCCAATGCCAACTGACCAACTGGCCATATTCGGAGCAATTTGAAGCCAATTT
CCATCGCCTGGCGATCGCTCCATTCTTGGCTATATGTTTTTCACCGTTTCCGGGGCCATTTTCAAAGACT
CGTCGGCAAGATAAGATTGTGTCACTCGCTGTCTCTCTTCATTTGTCGAAGAATGCTGAGGAATTTCGCG
ATGACGTCGGCGAGTATTTTGAAGAATGAGAATAATTTGTATTTATACGAAAATCAGTTAGTGGAATTTT
CTACAAAAACATGTTATCTATAGATAATTTTGTTGCAAAATATGTTGACTATGACAAAGATTGTATGTAT
ATACCTTTAATGTATTCTCATTTTCTTATGTATTTATAATGGCAATGATGATACTGATGATATTTTAAGA
TGATGCCAGACCAAAAGGCTTGAATTTCTGCGTCTTTTGCCGAACGCAGTGCATGTGCAATTGTTGTTTT
TTGGAATATTCAATTTTCGGACTGTCCGCTTTGATTTCAGTTTCTTGGCTTATTCAAAAAGCAAAGTAAA
GCCAAAAAAGCGAGATGGCAATACCAAATGCGGCAAAACGGTAGTGGAAGGAAAGGGGTGCGGGGCAGCG
GAAGGAAGGGTGGGGCGGGGCGTGGCGGGGTCTGTGGCTGGGCGCGACGTCACCGACGTTGGAGCCACTC
CTTTGACCATGTGTGCGTGTGTGTATTATTCGTGTCTCGCCACTCGCCGGTTGTTTTTTTCTTTTTATGC
TGCGCTCTCTCTAGCGCCATCTCGCTTACGCATGCTCAACGCACCGCATGTTGCCGTTTCCTTTTATGCG
TCATTTTGGCTCGAAATAGGCAATTATTTAAACAAAGATTAGTCAACGAAAACGCTAAAATAAATAAGTC
TACAATATGGTTACTTATTGCCATGTGTGTGCAGCCAACGATAGCAACAAAAGCAACAACACAGGTGGCT
TTCCCTCTTTCACTTTTTGTTTGCAAGCCGCGTGCGAGCAAGACGGCACGACCGGCAAACGCAATTACGC
TGACAAAGAGCAGACGAAGTTTTGGCGAAAAACATCAAGGCGCCTGATACGAATGCATTTGCAATAACAA
TTGCGATATTTAATATTGTTTATGAAGCTGTTTGACTTCAAAACACACAAAAAAAAAATAAAACAAATT
ATTTGAAAGAGAATTAGGAATCGGACGCTTATCGTTAGGGTAACAACAAGAAATGCTTACTGAGTCACAG
CCTCTGGAAAACTGCCGCAAGCCAGAGAGAGAGAGAAAAAGAGGGAGAGCAGCTTAGACCGCATGTGCTT
GTGTGTGAGGCGTCTCTCTCTTCGTCTCTGTTGCGCAAACGCATAGACTGCACTGAAAAAATCGATTACC
TATTTTTTATGAATGAATATTTGCACTATTACTATTCAAAACTATTAAGATAGCAATCACATTCAATAGC
CAAATACTATACCACCTGAGCGATGCAACGAAATGATCAATTTGAGCAAAAATGCTGCATATTTAGGACG
GCATCATTATAGAAATGCTTCTTGCTGTGTACTTTTCTCTCGTCTGGCAGCTGTTTCGCCGTTATTGTTA
AAACCGGCTTAAGTTAGGTGTGTTTTCTACGACTAGTGAATGCCCTACTAGAAGATGTGTGTTGCACAAA
ATGTCCCTGGAATAACCAATTTGAAGTGCAGATAGCAGTAAACGTAAGCTAATATGAATATTATTTAACT
GTAATGTTTTAATATCGCTGGACATTACTAATAAACCCACTATAAACACATGTACATATGTATGTTTTGG
CATACAATGAGTAGTTGGGGAAAAAATGTGTAAAAGCACCGTGACCATCACAGCATAAAGATAACCAGCT
GAAGTATCGAATATGAGTAACCCCCAAATTGAATCACATGCCGCAACTGATAGGACCCATGGAAGTACAC

TCTTCATGGCGATATACAAGACACACACAAGCACGAACACCCAGTTGCGGAGGAAATTCTCCGTAAATGA
AAACCCAATCGGCGAACAATTCATACCCATATATGGTAAAAGTTTTGAACGCGACTTGAGAGCGGAGAGC
ATTGCGGCTGATAAGGTTTTAGCGCTAAGCGGGCTTTATAAAACGGGCTGCGGGACCAGTTTTCATATCA
CTACCGTTTGAGTTCTTGTGCTGTGTGGATACTCCTCCCGACACAAAGCCGCTCCATCAGCCAGCAGTCG
TCTAATCCAGAGACCCCGGATCGGAAAAATGGACTGGTTACTAGCAACTCCGCAGTTGTACAGCGCGTTC
TCCTCCTTGGGTTGCTTGGAGGGCGATACCTATGTGGTCAACCCGAATGCATTGGCCATTCTGGAGGAGA
TCAACTACAAGCTCACCTATGAGGACCAAACACTGCGCACCTTTCGACGGGCCATTGGATTTGGCCAGAA
TGTGAGGTCAGACCTGATACCGCTGCTGGAGAATGCCAAGGATGATGCGGTCCTGGAGTCGGTCATCCGG
ATACTCGTCAATCTGACGGTGCCGGTGGAGTGCCTCTTCTCCGTGGACGTGATGTACCGCACGGATGTGG
GTCGCCACACCATCTTCGAGCTGAATAAGCTGCTGTACACCAGCAAGGAAGCATTTACCGAGGCCAGGAG
CACCAAGAGCGTGGTGGAGTACATGAAACACATACTGGAGTCGGACCCTAAGCTGTCGCCGCACAAATGC
GATCAAATCAACAACTGTCTGCTGCTGCTGAGAAATATCCTGCACATTCCAGAGACGCATGCCCATTGCG
TGATGCCCATGATGCAGTCGATGCCGCATGGCATCTCCATGCAGAACACGATCTTGTGGAATCTCTTCAT
CCAGAGCATCGACAAGTTACTCCTGTATCTGATGACCTGTCCGCAGAGAGCCTTCTGGGGAGTGACCATG
GTGCAACTGATTGCTTTGATCTACAAGGATCAGCATGTGAGCACTCTGCAAAAACTACTTAGCCTCTGGT
TCGAAGCCTCTCTGTCGGAGAGCTCTGAGGATAATGAGAGTAATACCTCGCCCCCCAAACAGGGCAGTGG
CGATTCCAGCCCCATGCTGACCTCTGATCCTACCTCTGATTCCTCGGACAATGGCAGCAATGGCCGTGGC
ATGGGCGGTGGCATGCGGGAAGGAACAGCGGCCACTTTGCAGGAGGTCAGCCGCAAGGGTCAGGAGTATC
AGAACGCCATGGCCAGAGTGCCAGCGGATAAGCCCGATGGCTCCGAAGAGGCCAGCGATATGACGGGGAA
CGACAGCGAGCAGCCTGGATCGCCGGAGCAATCGCAGCCCGCCGGCGAGTCCATGGATGATGGAGATTAC
GAGGACCAGAGACACAGGCAACTGAACGAGCATGGCGAAGAGGATGAAGATGAGGACGAAGTGGAGGAGG
AAGAGTACCTACAATTGGGCCCAGCCTCGGAGCCCCTAAACTTAACACAACAACCAGCTGACAAGGTCAA
CAACACTACCAACCCAACGTCCAGTGCGCCACAAGGCTGCCTGGGCAATGAGCCATTCAAGCCACCACCT
CCTCTGCCAGTCAGAGCCTCCACCTCGGCACACGCTCAAATGCAGAAGTTCAACGAATCGTCCTACGCGT
CCCACGTATCTGCGGTCAAATTGGGCCAAAAGTCCCCACATGCCGGCCAGCTCCAGCTGACCAAGGGCAA
GTGTTGTCCACAGAAGCGGGAATGCCCCTCCTCGCAGTCGGAGCTATCGGATTGCGGTTATGGCACCCAG
GTGGAAAATCAGGAATCCATTTCCACCTCCAGCAACGACGATGATGGGCCGCAGGGCAAGCCGCAGCACC
AGAAGCCTCCGTGTAACACGAAGCCACGGAATAAACCACGGACGATTATGTCGCCAATGGACAAAAAGGA
GCTTAGACGCAAAAAACTGGTCAAGCGCAGCAAAAGCAGCCTCATCAACATGAAGGGTCTGGTACAGCAC
ACCCCCACCGATGATGACATCTCCAATCTGCTGAAGGAATTCACCGTGGATTTCCTCCTCAAGGGTTACA
GCTATCTGGTGGAGGAACTGCACATGCAACTGCTTTCCAATGCGAAGGTGCCCATTGACACATCGCACTT
CTTCTGGCTGGTCACCTACTTCCTGAAGTTTGCCGCCCAACTGGAGCTGGATATGGAGCACATCGACACT
ATTCTCACCTACGATGTTTTGAGCTACTTGACCTATGAGGGTGTGTCCCTATGTGAGCAACTGGAACTGA
ATGCCCGACAGGAGGGCAGTGACCTGAAGCCCTATCTAAGGCGAATGCACTTGGTGGTGACGGCCATCCG
GGAGTTCCTCCAGGCCATTGATACGTACAACAAAGTGACTCATCTGAACGAGGACGACAAAGCCCATTTG
AGGCAGCTTCAGCTGCAGATTAGCGAAATGTCCGATCTGAGGTGCCTTTTTGTGCTTCTGCTGAGGCGTT
TCAATCCCAGCATTCATTCCAAGCAGTATCTTCAGGATCTGGTGGTTACCAATCACATCCTCCTACTCAT
TCTGGACAGTTCGGCCAAACTTGGTGGATGTCAAACCATTCGCCTGTCGGAGCACATTACACAGTTTGCC
ACGCTGGAGGTGATGCACTACTATGGCATTCTGTTGGAGGACTTCAACAACAACGGAGAGTTTGTCAATG
ACTGCATCTTCACCATGATGCATCACATCGGTGGCGATCTGGGCCAGATTGGGGTTCTATTTCAACCAAT
TATTTTGAAAACCTATTCAAGAATTTGGGAAGCGGACTATGAACTGTGCGATGACTGGTCTGATCTTATC
GAGTATGTGATTCACAAGTTCATGAATACTCCTCCGAAGTCGCCACTCACCATTCCTACAACTTCCTTGA
CGGAAATGACCAAGGAACACAACCAGGAGCATACCGTTTGCTCTTGGTCGCAGGAGGAAATGGACACACT
TTATTGGTATTATGTGCAGAGCAAGAAGAACAACGATATTGTGGGAAAGATAGTTAAGCTCTTCAGCAAC
AACGGCAACAAGCTGAAAACCAGGATTTCTATTATCCAACAACTTTTGCAACAAGACATTATCACCCTGT
TGGAATACGATGACCTGATGAAGTTCGAGGATGCGGAGTATCAGAGAACTTTGCTGACAACTCCCACTTC
CGCAACAACAGAGTCTGGAATTGAGATTAAGGAGTGCGCCTACGGCAAACCCTCAGATGATGTTCAGATC
CTGCTGGACCTGATCATTAAGGAAAACAAGGCGCAGCATTTGTTATGGCTGCAAAGGATCCTCATTGAGT
GCTGCTTCGTTAAACTGACCCTGCGGAGTGGTCTCAAGGTTCCGGAAGGCGATCACATCATGGAGCCGGT
GGCCTACCACTGCATCTGCAAGCAGAAGTCCATTCCGGTGGTGCAGTGGAACAACGAGCAATCCACTACG
ATGCTGTACCAGCCTTTTGTTCTCCTGCTCCACAAGCTGGGCATTCAGCTGCCGGCGGACGCGGGCTCGA
TCTTCGCCAGAATTCCGGACTACTGGACACCGGAGACAATGTACGGACTCGCCAAAAAGCTGGGACCGCT
GGACAAACTCAACCTCAAGTTCGACGCCAGTGAACTGGAGGATGCGACGGCGTCGAGTCCGTCGCGTTAC

CACCACACCGGACCCCGCAACTCGCTCAGCTCGGTAAGCAGCCTGGACGTGGATCTCGGCGATACCGAGG
AGCTGGCCCTTATACCCGAGGTGGATGCGGCCGTGGAGAAGGCACACGCCATGGCATCCACGCCATCGCC
CAGCGAGATTTTCGCGGTTCCCAAGACGAAGCACTGCAACTCGATCATCAGATACACACCAGATCCCACG
CCTCCAGTGCCCAACTGGCTGCAGTTGGTCATGCGCAGCAAATGCAATCATCGCACAGGTCCGTCTGGTG
ATCCCAGCGATTGCATTGGCTCCTCGTCGACAACCGTGGACGATGAGGGATTTGGCAAGTCCATCAGTGC
AGCCACTTCGCAGGCGGCGAGCACCTCCATGAGCACGGTTAATCCCACAACCACTTTGAGCCTGAACATG
CTAAACACCTTCATGGGAAGCCACAACGAGAACAGCAGCAGTTCTGGTTGCGGGGGCACCGTCTCCTCCC
TGTCCATGGTGGCTCTGATGAGCACCGGCGCGGCAGGCGGAGGAGGTAACACCTCCGGGCTGGAAATGGA
TGTGGACGCCTCCATGAAGTCCTCGTTCGAGCGGCTGGAGGTAAACGGATCGCACTTCTCGCGGGCCAAC
AACTTGGACCAGGAGTACAGTGCCATGGTGGCATCTGTGTACGAAAAGGAGAAGGAATTAAACAGCGACA
ATGTCTCTTTGGCCTCGGACCTGACCAGAATGTATGTGAGCGATGAGGACGATCGACTTGAGCGAACCGA
GATCCGGGTGCCCCACTATCACCTCGAGGGTGGCTCAGGAATGGACAAAGACTGCGAAATGAAGCGCACC
ACCCTGGATAGCCCTCTGGGCAAGCTGGAACTGTCTGGGTGCGAACAGGGCCTGCACCGTATCATCTTCC
TGGGCAAAGGAACATCTGCCGCCGACGCCGTGGAAGTGCCTGCCCCAGCCGCCGTGCTGGGCGGACCAGA
GCCACTGATGCAGGCCACCGCCTGGCTCAACGCCTACTTTCACCAGCCTGAGGCCATCGAGGAGTTCCCT
GTGCCAGCCCTGCACCACCCAGTGTTCCAGCAGGAGAGCTTTACCCGCCAGGTGCTGTGGAAACTGCTGA
AAGTGGTGAAGTTCGGAGAGGTCATCAGCTACAGCCACCTGGCCGCCCTGGCCGGCAATCCCGCCGCCAC
CGCCGCCGTGAAAACCGCCCTGAGCGGAAATCCCGTGCCCATTCTGATCCCCTGCCACCGGGTGGTGCAG
GGCGACCTGGACGTGGGGGGCTACGAGGGCGGGCTCGCCGTGAAAGAGTGGCTGCTGGCCCACGAGGGCC
ACAGACTGGGCAAGCCTGGGCTGGGTGGGGGCGGGTACCCATACGATGTTCCAGATTACGCTCGTACCGG
TGGTGGCTCGGGAAGCCGCCTGGAAGAAGAACTGCGCCGCCGCCTGACCGAATGAGTTTAAACCCGCTGA
TCAGCCTCGACTGTGCCTTCTAAGGCCTGAGCTAGCTGATCAGCCTCGATCGAGGGATCCAGACATGATA
AGATACATTGATGAGTTTGGACAAACCACAACTAGAATGCAGTGAAAAAAATGCTTTATTTGTGAAATTT
GTGATGCTATTGCTTTATTTGTAACCATTATAAGCTGCAATAAACAAGTTAACAACAACAATTGCATTCA
TTTTATGTTTCAGGTTCAGGGGGAGGTGTGGGAGGTTTTTTAAAGCAAGTAAAACCTCTACAAATGTGGT
ATGGCTGATTATGATCAGTCGACCGATGCCCTTGAGAGCCTTCAACCCAGTCAGCTCCTTCCGGTGGGCG
CGGGGCATGACTATCGTCGCCGCACTTATGACTGTCTTCTTTATCATGCAACTCGTAGGACAGGTGCCGG
CAGCGCTCTGGGTCATTTTCGGCGAGGACCGCTTTCGCTGGAGCGCGACGATGATCGGCCTGTCGCTTGC
GGTATTCGGAATCTTGCACGCCCTCGCTCAAGCCTTCGTCACTGGTCCCGCCACCAAACGTTTCGGCGAG
AAGCAGGCCATTATCGCCGGCATGGCGGCCGACGCGCTGGGCTACGTCTTGCTGGCGTTCGCGACGCGAG
GCTGGATGGCCTTCCCCATTATGATTCTTCTCGCTTCCGGCGGCATCGGGATGCCCGCGTTGCAGGCCAT
GCTGTCCAGGCAGGTAGATGACGACCATCAGGGACAGCTTCAAGGCCAGCAAAAGGCCAGGAACCGTAAA
AAGGCCGCGTTGCTGGCGTTTTTCCATAGGCTCCGCCCCCCTGACGAGCATCACAAAAATCGACGCTCAA
GTCAGAGGTGGCGAAACCCGACAGGACTATAAAGATACCAGGCGTTTCCCCCTGGAAGCTCCCTCGTGCG
CTCTCCTGTTCCGACCCTGCCGCTTACCGGATACCTGTCCGCCTTTCTCCCTTCGGGAAGCGTGGCGCTT
TCTCATAGCTCACGCTGTAGGTATCTCAGTTCGGTGTAGGTCGTTCGCTCCAAGCTGGGCTGTGTGCACG
AACCCCCCGTTCAGCCCGACCGCTGCGCCTTATCCGGTAACTATCGTCTTGAGTCCAACCCGGTAAGACA
CGACTTATCGCCACTGGCAGCAGCCACTGGTAACAGGATTAGCAGAGCGAGGTATGTAGGCGGTGCTACA
GAGTTCTTGAAGTGGTGGCCTAACTACGGCTACACTAGAAGGACAGTATTTGGTATCTGCGCTCTGCTGA
AGCCAGTTACCTTCGGAAAAAGAGTTGGTAGCTCTTGATCCGGCAAACAAACCACCGCTGGTAGCGGTGG
TTTTTTTGTTTGCAAGCAGCAGATTACGCGCAGAAAAAAAGGATCTCAA

CLIP-CRYΔ in pAC5.1 vector backbone (with unintentional minor differences from standard pAC5.1)

Key features:
Ampicillin Resistance: 171-1136
Actin 5C promoter: 1286-3794
Drosophila Kozak sequence: 3807-3814
3X myc-tag: 3814-3921

CLIP-tag: 3931-4476
CRY△: 4489-6048
Replication origin: 6944-7532

GAAGATCCTTTGATCTTTTCTACGGGGTCTGACGCTCAGTGGAACGAAAACTCACGTTAAGGGATTTTGG
TCATGAGATTATCAAAAAGGATCTTCACCTAGATCCTTTTAAATTAAAAATGAAGTTTTAAATCAATCTA
AAGTATATATGAGTAAACTTGGTCTGACAGTTACCAATGCTTAATCAGTGAGGCACCTATCTCAGCGATC
TGTCTATTTCGTTCATCCATAGTTGCCTGACTCCCCGTCGTGTAGATAACTACGATACGGGAGGGCTTAC
CATCTGGCCCCAGTGCTGCAATGATACCGCGAGACCCACGCTCACCGGCTCCAGATTTATCAGCAATAAA
CCAGCCAGCCGGAAGGGCCGAGCGCAGAAGTGGTCCTGCAACTTTATCCGCCTCCATCCAGTCTATTAAT
TGTTGCCGGGAAGCTAGAGTAAGTAGTTCGCCAGTTAATAGTTTGCGCAACGTTGTTGCCATTGCTGCAG
GCATCGTGGTGTCACGCTCGTCGTTTGGTATGGCTTCATTCAGCTCCGGTTCCCAACGATCAAGGCGAGT
TACATGATCCCCCATGTTGTGCAAAAAAGCGGTTAGCTCCTTCGGTCCTCCGATCGTTGTCAGAAGTAAG
TTGGCCGCAGTGTTATCACTCATGGTTATGGCAGCACTGCATAATTCTCTTACTGTCATGCCATCCGTAA
GATGCTTTTCTGTGACTGGTGAGTACTCAACCAAGTCATTCTGAGAATAGTGTATGCGGCGACCGAGTTG
CTCTTGCCCGGCGTCAACACGGGATAATACCGCGCCACATAGCAGAACTTTAAAAGTGCTCATCATTGGA
AAACGTTCTTCGGGGCGAAAACTCTCAAGGATCTTACCGCTGTTGAGATCCAGTTCGATGTAACCCACTC
GTGCACCCAACTGATCTTCAGCATCTTTTACTTTCACCAGCGTTTCTGGGTGAGCAAAAACAGGAAGGCA
AAATGCCGCAAAAAAGGGAATAAGGGCGACACGGAAATGTTGAATACTCATACTCTTCCTTTTTCAATAT
TATTGAAGCATTTATCAGGGTTATTGTCTCATGAGCGGATACATATTTGAATGTATTTAGAAAAATAAAC
AAATAGGGGTTCCGCGCACATTTCCCCGAAAAGTGCCACCTGACGTCTAAGAAACCATTATTATCATGAC
ATTAACCTATAAAAATAGGCGTATCACGAGGCCCTTTCGTCTTCAAGAATTAATTCTATATTCTAAAAAC
ACAAATGATACTTCTAAAAAAAAATCATGAATGGCATCAACTCTGAATCAAATCTTTGCAGATGCACCTA
CTTCTCATTTCCACTGTCACATCATTTTTCCAGATCTCGCTGCCTGTTATGTGGCCCACAAACCAAGACA
CGTTTTATGGCCATTAAAGCTGGCTGATCGTCGCCAAACACCAAATACATAATGAATATGTACACATTCG
AGAAAGAAGCGATCAAAGAAGCGTCTTCGGGCGGAGTAGGAGAATGCGGAGGAGAAGGAGAACGAGCTGA
TCTAGTATCTCTCCACAATCCAATGCCAACTGACCAACTGGCCATATTCGGAGCAATTTGAAGCCAATTT
CCATCGCCTGGCGATCGCTCCATTCTTGGCTATATGTTTTTCACCGTTTCCGGGGCCATTTTCAAAGACT
CGTCGGCAAGATAAGATTGTGTCACTCGCTGTCTCTCTTCATTTGTCGAAGAATGCTGAGGAATTTCGCG
ATGACGTCGGCGAGTATTTTGAAGAATGAGAATAATTTGTATTTATACGAAAATCAGTTAGTGGAATTTT
CTACAAAAACATGTTATCTATAGATAATTTTGTTGCAAAATATGTTGACTATGACAAAGATTGTATGTAT
ATACCTTTAATGTATTCTCATTTTCTTATGTATTTATAATGGCAATGATGATACTGATGATATTTTAAGA
TGATGCCAGACCAAAAGGCTTGAATTTCTGCGTCTTTTGCCGAACGCAGTGCATGTGCAATTGTTGTTTT
TTGGAATATTCAATTTTCGGACTGTCCGCTTTGATTTCAGTTTCTTGGCTTATTCAAAAAGCAAAGTAAA
GCCAAAAAAGCGAGATGGCAATACCAAATGCGGCAAAACGGTAGTGGAAGGAAAGGGGTGCGGGGCAGCG
GAAGGAAGGGTGGGGCGGGGCGTGGCGGGGTCTGTGGCTGGGCGCGACGTCACCGACGTTGGAGCCACTC
CTTTGACCATGTGTGCGTGTGTGTATTATTCGTGTCTCGCCACTCGCCGGTTGTTTTTTTCTTTTTATGC
TGCGCTCTCTCTAGCGCCATCTCGCTTACGCATGCTCAACGCACCGCATGTTGCCGTTTCCTTTTATGCG
TCATTTTGGCTCGAAATAGGCAATTATTTAAACAAAGATTAGTCAACGAAAACGCTAAAATAAATAAGTC
TACAATATGGTTACTTATTGCCATGTGTGTGCAGCCAACGATAGCAACAAAAGCAACAACACAGGTGGCT
TTCCCTCTTTCACTTTTTGTTTGCAAGCCGCGTGCGAGCAAGACGGCACGACCGGCAAACGCAATTACGC
TGACAAAGAGCAGACGAAGTTTTGGCGAAAAACATCAAGGCGCCTGATACGAATGCATTTGCAATAACAA
TTGCGATATTTAATATTGTTTATGAAGCTGTTTGACTTCAAAACACACAAAAAAAAAAATAAAACAAATT
ATTTGAAAGAGAATTAGGAATCGGACGCTTATCGTTAGGGTAACAACAAGAAATGCTTACTGAGTCACAG
CCTCTGGAAAACTGCCGCAAGCCAGAGAGAGAGAGAAAAAGAGGGAGAGCAGCTTAGACCGCATGTGCTT
GTGTGTGAGGCGTCTCTCTCTTCGTCTCTGTTGCGCAAACGCATAGACTGCACTGAAAAAATCGATTACC
TATTTTTTATGAATGAATATTTGCACTATTACTATTCAAAACTATTAAGATAGCAATCACATTCAATAGC
CAAATACTATACCACCTGAGCGATGCAACGAAATGATCAATTTGAGCAAAAATGCTGCATATTTAGGACG
GCATCATTATAGAAATGCTTCTTGCTGTGTACTTTTCTCTCGTCTGGCAGCTGTTTCGCCGTTATTGTTA
AAACCGGCTTAAGTTAGGTGTGTTTTCTACGACTAGTGAATGCCCTACTAGAAGATGTGTGTTGCACAAA
ATGTCCCTGGAATAACCAATTTGAAGTGCAGATAGCAGTAAACGTAAGCTAATATGAATATTATTTAACT
GTAATGTTTTAATATCGCTGGACATTACTAATAAACCCACTATAAACACATGTACATATGTATGTTTTGG
CATACAATGAGTAGTTGGGGAAAAAATGTGTAAAAGCACCGTGACCATCACAGCATAAAGATAACCAGCT

GAAGTATCGAATATGAGTAACCCCCAAATTGAATCACATGCCGCAACTGATAGGACCCATGGAAGTACAC
TCTTCATGGCGATATACAAGACACACACAAGCACGAACACCCAGTTGCGGAGGAAATTCTCCGTAAATGA
AAACCCAATCGGCGAACAATTCATACCCATATATGGTAAAAGTTTTGAACGCGACTTGAGAGCGGAGAGC
ATTGCGGCTGATAAGGTTTTAGCGCTAAGCGGGCTTTATAAAACGGGCTGCGGGACCAGTTTTCATATCA
CTACCGTTTGAGTTCTTGTGCTGTGTGGATACTCCTCCCGACACAAAGCCGCTCCATCAGCCAGCAGTCG
TCTAATCCAGAGACCCCGGATCGGGGAAAAATGGAGCAGAAGCTGATCTCAGAGGAGGACCTGGGAGGAG
GAGAACAAAAATTAATAAGTGAAGAAGACCTGGGCGGCGGCGAGCAGAAGCTGATCTCAGAGGAGGACCT
GGGAGGAGGAATGGACAAAGACTGCGAAATGAAGCGCACCACCCTGGATAGCCCTCTGGGCAAGCTGGAA
CTGTCTGGGTGCGAACAGGGCCTGCACCGTATCATCTTCCTGGGCAAAGGAACATCTGCCGCCGACGCCG
TGGAAGTGCCTGCCCCAGCCGCCGTGCTGGGCGGACCAGAGCCACTGATCCAGGCCACCGCCTGGCTCAA
CGCCTACTTTCACCAGCCTGAGGCCATCGAGGAGTTCCCTGTGCCAGCCCTGCACCACCCAGTGTTCCAG
CAGGAGAGCTTTACCCGCCAGGTGCTGTGGAAACTGCTGAAAGTGGTGAAGTTCGGAGAGGTCATCAGCG
AGAGCCACCTGGCCGCCCTGGTGGGCAATCCCGCCGCCACCGCCGCCGTGAACACCGCCCTGGACGGAAA
TCCCGTGCCCATTCTGATCCCCTGCCACCGGGTGGTGCAGGGCGACAGCGACGTGGGGCCCTACCTGGGC
GGGCTCGCCGTGAAAGAGTGGCTGCTGGCCCACGAGGGCCACAGACTGGGCAAGCCTGGGCTGGGTGGTG
GCTCAGGAATGGCCACGCGAGGGGCGAATGTGATTTGGTTTCGCCATGGATTGCGCCTCCATGATAATCC
CGCTCTATTGGCCGCCCTCGCCGATAAGGATCAGGGTATAGCCCTAATTCCCGTTTTCATATTCGATGGA
GAGAGTGCAGGTACCAAGAATGTGGGTTACAATCGGATGCGTTTCCTCCTGGACTCGTTGCAGGACATCG
ATGATCAGCTACAGGCGGCAACTGATGGACGTGGACGCCTCCTGGTCTTCGAGGGCGAACCGGCTTATAT
CTTCCGCCGGCTACATGAGCAAGTGCGTCTGCACAGGATTTGCATAGAGCAGGACTGCGAGCCAATTTGG
AATGAGCGCGATGAAAGCATCCGTTCTCTATGTCGGGAGCTGAATATCGACTTTGTCGAGAAGGTATCAC
ACACGCTTTGGGATCCGCAATTGGTGATTGAGACCAATGGTGGCATTCCACCGCTGACCTACCAAATGTT
CCTGCACACGGTGCAAATTATTGGGCTTCCACCGCGTCCCACCGCCGATGCTCGACTAGAAGACGCCACC
TTTGTCGAGCTGGACCCCGAGTTCTGCCGAAGTCTTAAGTTGTTCGAGCAGCTGCCCACGCCGGAGCACT
TCAATGTGTATGGAGACAACATGGGCTTCCTGGCCAAGATTAACTGGCGCGGCGGAGAAACACAGGCCTT
ACTTCTGTTGGATGAGCGTCTTAAAGTGGAGCAGCATGCGTTTGAGCGTGGATTTTATCTGCCCAACCAG
GCACTGCCCAATATCCACGACTCGCCAAAATCGATGAGCGCCCATCTGCGCTTTGGTTGCCTTTCGGTAC
GTCGCTTCTACTGGAGCGTCCACGATCTCTTCAAGAATGTCCAGTTGCGCGCCTGTGTGCGGGGCGTTCA
GATGACTGGCGGCGCGCACATCACGGGACAGTTGATCTGGCGAGAGTACTTCTACACCATGTCGGTGAAC
AATCCAAACTACGATCGCATGGAGGGCAATGACATCTGCCTGAGCATCCCGTGGGCTAAGCCGAACGAAA
ATCTCCTGCAGAGCTGGCGTTTAGGCCAAACGGGATTCCCGCTCATCGACGGCGCCATGCGACAACTCCT
GGCCGAGGGATGGCTCCACCATACGCTGCGCAACACCGTGGCCACCTTTCTCACGCGCGGCGGTTTGTGG
CAGAGCTGGGAGCATGGACTGCAGCACTTTCTGAAGTATCTGCTGGATGCGGATTGGTCGGTCTGCGCTG
GCAACTGGATGTGGGTATCCAGCTCGGCGTTTGAAAGGCTGCTGGACTCCTCCCTGGTCACCTGCCCGGT
GGCATTGGCCAAGCGACTTGATCCGGATGGCACCTACATCAAGCAGTACGTCCCGGAGTTGATGAATGTG
CCCAAGGAATTTGTTCACGAGCCCTGGCGAATGTCTGCCGAGCAGCAGGAGCAGTACGAGTGCCTGATCG
GAGTCCATTATCCGGAGCGGATCATTGATTTGTCCATGGCCGTAAAGCGAAACATGCTGGCCATGAAGTC
TCTCCGAAATTCGCTGATCACCCCGCCGTAATCTAGAGGGCCCTTCGAAGGTAAGCCTATCCCTAACCCT
CTCCTCGGTCTCGATTCTACGCGTACCGGTCATCATCACCATCACCATTGAGTTTAAACCCGCTGATCAG
CCTCGACTGTGCCTTCTAAGGCCTGAGCTAGCTGATCAGCCTCGATCGAGGATCCAGACATGATAAGATA
CATTGATGAGTTTGGACAAACCACAACTAGAATGCAGTGAAAAAAATGCTTTATTTGTGAAATTTGTGAT
GCTATTGCTTTATTTGTAACCATTATAAGCTGCAATAAACAAGTTAACAACAACAATTGCATTCATTTTA
TGTTTCAGGTTCAGGGGGAGGTGTGGGAGGTTTTTTAAAGCAAGTAAAACCTCTACAAATGTGGTATGGC
TGATTATGATCAGTCGACCGATGCCCTTGAGAGCCTTCAACCCAGTCAGCTCCTTCCGGTGGGCGCGGGG
CATGACTATCGTCGCCGCACTTATGACTGTCTTCTTTATCATGCAACTCGTAGGACAGGTGCCGGCAGCG
CTCTGGGTCATTTTCGGCGAGGACCGCTTTCGCTGGAGCGACGATGATCGGCCTGTCGCTTGCGGTATTC
GGAATCTTGCACGCCCTCGCTCAAGCCTTCGTCACTGGTCCCGCCACCAAACGTTTCGGCGAGAAGCAGG
CCATTATCGCCGGCATGGCGGCCGACGCGCTGGGCTACGTCTTGCTGGCGTTCGCGACGCGAGGCTGGAT
GGCCTTCCCCATTATGATTCTTCTCGCTTCCGGCGGCATCGGGATGCCCGCGTTGCAGGCCATGCTGTCC
AGGCAGGTAGATGACGACCATCAGGGACAGCTTCAAGGCCAGCAAAAGGCCAGGAACCGTAAAAAGGCCG
CGTTGCTGGCGTTTTTCCATAGGCTCCGCCCCCCTGACGAGCATCACAAAAATCGACGCTCAAGTCAGAG
GTGGCGAAACCCGACAGGACTATAAAGATACCAGGCGTTTCCCCCTGGAAGCTCCCTCGTGCGCTCTCCT
GTTCCGACCCTGCCGCTTACCGGATACCTGTCCGCCTTTCTCCCTTCGGGAAGCGTGGCGCTTTCTCATA

GCTCACGCTGTAGGTATCTCAGTTCGGTGTAGGTCGTTCGCTCCAAGCTGGGCTGTGTGCACGAACCCCC
CGTTCAGCCCGACCGCTGCGCCTTATCCGGTAACTATCGTCTTGAGTCCAACCCGGTAAGACACGACTTA
TCGCCACTGGCAGCAGCCACTGGTAACAGGATTAGCAGAGCGAGGTATGTAGGCGGTGCTACAGAGTTCT
TGAAGTGGTGGCCTAACTACGGCTACACTAGAAGGACAGTATTTGGTATCTGCGCTCTGCTGAAGCCAGT
TACCTTCGGAAAAAGAGTTGGTAGCTCTTGATCCGGCAAACAAACCACCGCTGGTAGCGGTGGTTTTTTT
GTTTGCAAGCAGCAGATTACGCGCAGAAAAAAAGGATCTCAA

Proteins Sequences:

CLIP-CRYΔ (MW = 83.7 kDa)

MEQKLISEEDLGGGEQKLISEEDLGGGEQKLISEEDLGGGMDKDCEMKRTTLDSPLGKLELSGC
EQGLHRIIFLGKGTSAADAVEVPAPAAVLGGPEPLIQATAWLNAYFHQPEAIEEFPVPALHHPV
FQQESFTRQVLWKLLKVVKFGEVISESHLAALVGNPAATAAVNTALDGNPVPILIPCHRVVQGD
SDVGPYLGGLAVKEWLLAHEGHRLGKPGLGGGSGMATRGANVIWFRHGLRLHDNPALLAALADK
DQGIALIPVFIFDGESAGTKNVGYNRMRFLLDSLQDIDDQLQAATDGRGRLLVFEGEPAYIFRR
LHEQVRLHRICIEQDCEPIWNERDESIRSLCRELNIDFVEKVSHTLWDPQLVIETNGGIPPLTY
QMFLHTVQIIGLPPRPTADARLEDATFVELDPEFCRSLKLFEQLPTPEHFNVYGDNMGFLAKIN
WRGGETQALLLLDERLKVEQHAFERGFYLPNQALPNIHDSPKSMSAHLRFGCLSVRRFYWSVHD
LFKNVQLRACVRGVQMTGGAHITGQLIWREYFYTMSVNNPNYDRMEGNDICLSIPWAKPNENLL
QSWRLGQTGFPLIDGAMRQLLAEGWLHHTLRNTVATFLTRGGLWQSWEHGLQHFLKYLLDADWS
VCAGNWMWVSSSAFERLLDSSLVTCPVALAKRLDPDGTYIKQYVPELMNVPKEFVHEPWRMSAE
QQEQYECLIGVHYPERIIDLSMAVKRNMLAMKSLRNSLITPP

TIM-SNAP-HA-ALFA (MW = 179.8 kDa)

MDWLLATPQLYSAFSSLGCLEGDTYVVNPNALAILEEINYKLTYEDQTLRTFRRAIGFGQNVRS
DLIPLLENAKDDAVLESVIRILVNLTVPVECLFSVDVMYRTDVGRHTIFELNKLLYTSKEAFTE
ARSTKSVVEYMKHILESDPKLSPHKCDQINNCLLLLRNILHIPETHAHCVMPMMQSMPHGISMQ
NTILWNLFIQSIDKLLLYLMTCPQRAFWGVTMVQLIALIYKDQHVSTLQKLLSLWFEASLSESS
EDNESNTSPPKQGSGDSSPMLTSDPTSDSSDNGSNGRGMGGGMREGTAATLQEVSRKGQEYQNA
MARVPADKPDGSEEASDMTGNDSEQPGSPEQSQPAGESMDDGDYEDQRHRQLNEHGEEDEDEDE
VEEEEYLQLGPASEPLNLTQQPADKVNNTTNPTSSAPQGCLGNEPFKPPPPLPVRASTSAHAQM
QKFNESSYASHVSAVKLGQKSPHAGQLQLTKGKCCPQKRECPSSQSELSDCGYGTQVENQESIS
TSSNDDDGPQGKPQHQKPPCNTKPRNKPRTIMSPMDKKELRRKKLVKRSKSSLINMKGLVQHTP
TDDDISNLLKEFTVDFLLKGYSYLVEELHMQLLSNAKVPIDTSHFFWLVTYFLKFAAQLELDME
HIDTILTYDVLSYLTYEGVSLCEQLELNARQEGSDLKPYLRRMHLVVTAIREFLQAIDTYNKVT
HLNEDDKAHLRQLQLQISEMSDLRCLFVLLLRRFNPSIHSKQYLQDLVVTNHILLLILDSSAKL
GGCQTIRLSEHITQFATLEVMHYYGILLEDFNNNGEFVNDCIFTMMHHIGGDLGQIGVLFQPII
LKTYSRIWEADYELCDDWSDLIEYVIHKFMNTPPKSPLTIPTTSLTEMTKEHNQEHTVCSWSQE
EMDTLYWYYVQSKKNNDIVGKIVKLFSNNGNKLKTRISIIQQLLQQDIITLLEYDDLMKFEDAE
YQRTLLTTPTSATTESGIEIKECAYGKPSDDVQILLDLIIKENKAQHLLWLQRILIECCFVKLT
LRSGLKVPEGDHIMEPVAYHCICKQKSIPVVQWNNEQSTTMLYQPFVLLLHKLGIQLPADAGSI
FARIPDYWTPETMYGLAKKLGPLDKLNLKFDASELEDATASSPSRYHHTGPRNSLSSVSSLDVD
LGDTEELALIPEVDAAVEKAHAMASTPSPSEIFAVPKTKHCNSIIRYTPDPTPPVPNWLQLVMR
SKCNHRTGPSGDPSDCIGSSSTTVDDEGFGKSISAATSQAASTSMSTVNPTTTLSLNMLNTFMG
SHNENSSSSGCGGTVSSLSMVALMSTGAAGGGGNTSGLEMDVDASMKSSFERLEVNGSHFSRAN

NLDQEYSAMVASVYEKEKELNSDNVSLASDLTRMYVSDEDDRLERTEIRVPHYHLEGGSGMDKD
CEMKRTTLDSPLGKLELSGCEQGLHRIIFLGKGTSAADAVEVPAPAAVLGGPEPLMQATAWLNA
YFHQPEAIEEFPVPALHHPVFQQESFTRQVLWKLLKVVKFGEVISYSHLAALAGNPAATAAVKT
ALSGNPVPILIPCHRVVQGDLDVGGYEGGLAVKEWLLAHEGHRLGKPGLGGGGYPYDVPDYART
GGGSGSRLEEELRRRLTE

Supplementary Table 1. Cryo-EM data collection, refinement, and validation statistics

	CRY:TIM complex (EMDB-27335) (PDB 8DD7)
Data collection and processing	
Magnification	x79k
Voltage (kV)	200
Electron exposure (e–/Å^2)	53
Defocus range (μm)	-0.8 ~ -2.0
Pixel size (Å)	1.032
Symmetry imposed	C1
Initial particle images (no.)	334,787
Final particle images (no.)	159,544
Map resolution (Å)	3.3
FSC threshold	0.143
Map resolution range (Å)	2.4-5.5
Refinement	
Initial model used (PDB code)	4GU5
Model resolution (Å)	3.3
FSC threshold	0.143
Model resolution range (Å)	2.4-5.5
Map sharpening *B* factor (Å^2)	-122.7
Model composition	
Non-hydrogen atoms	10370
Protein residues	1275
Ligands	FAD: 1
B factors (Å^2)	
Protein	132
Ligand	58
R.m.s. deviations	
Bond lengths (Å)	0.006 (6)
Bond angles (°)	1.185 (10)
Validation	
MolProbity score	2.00
Clashscore	11.07
Poor rotamers (%)	0.44
Ramachandran plot	
Favored (%)	93.27
Allowed (%)	6.73
Disallowed (%)	0.00